Chapter 2: ZnO Nanostructures-An Overview

2.1 Preliminaries

Zinc Oxide is found in nature as the mineral Zincite [1], 'Zincum Oxydatum' is the Latin name of Zinc Oxide and it is commonly used in homeopathic medicines. The chemical formula of Zinc oxide is ZnO. Zinc oxide is a type of material which exhibits semiconducting and piezoelectric dual properties (in its crystalline form). Zinc Oxide is a 'direct band gap' and wurtzite (hexagonal) type semiconductor; it has band gap energy of 3.37 eV at room temperature. It is insoluble in water but easily soluble in acids and alkalis. It is also thermo chromic i.e. it changes color when heated (from white to yellow) and regains the original color when cooled down. When Zinc Oxide comes in contact with air it forms, a nervous malady called metal fume fever. The ZnO nanostructure has many applications in optoelectronics, sensors, and transducers and in the biomedical field. ZnO nanobelts can also be used as nanosensors, nanocantilivers, field effect transistors and nanoresonators. The lack of centre of symmetry in wurtzite combined with large electrochemical coupling, results in strong piezoelectric and pyroelectric properties. Consequently, ZnO is used in mechanical actuators and piezoelectric sensors. Due to its wide band gap, it is suitable for short wavelength optoelectronic applications.

The chemical formula of Zinc oxide is ZnO. Zinc oxide is an important material for a variety of practical applications; therefore, it has been under intensive investigation since the 1950s [2]. It is used as a pigment in paints, filler for rubber goods, in coatings for paper, as safe food additives and drugs [3]. Zinc peroxide, ZnO2·1/2H2O, is used in antiseptic ointments. Zinc oxide is also a semiconductor with a direct band gap of ~3.3 eV (387 nm, deep violet/borderline UV) which make it a possible candidate as a white light source when combined with certain types of phosphors by comparison (current light sources consume more than 20% of world electricity) [4]. Such solid-state light sources offer huge advantages in energy efficiency. Because of the wide band gap, zinc oxide absorbs ultraviolet light; thus, it can be used in ointments, creams and lotions to protect against sunburn. However, in terms of future use, the major interest lays in semiconductor applications, due to the increasing need for near-ultra-violet optoelectronic devices. ZnO is a candidate for solid state 'blue to UV optoelectronics', including lasers. Its light sensitivity makes it a potential detector of radiation in the UV spectrum. Crystalline zinc oxide also exhibits the piezoelectric effect.

2.2 Research Directions

Research on the properties of bulk ZnO has been going on for quite a long time and it has found a number of uses within a variety of common products. On a day to day basis, most people probably come into contact with

ISBN: 978-81-942709-0-4
Thesis DOI: 10.21467/thesis.78

Series: AIJR Thesis

it in sun screen and calamine lotion. The reason for its prominent use in sun screen goes back to the previously mentioned fact that it is transparent in visible spectrum and that it absorbs both UV A and UV B light. The more high-tech uses of ZnO have been in gas sensors and in the last couple of years blue LEDs. ZnO phosphors in the form of powders have in the past been the main focus of the scientific community. The ZnO phosphors usually appear as a strong green and efforts were to determine the origin of this color. A few reports would occasionally describe the appearance of other colors, such as red, which today are sometimes seen in nanostructures as well. From this point onwards research began into the creation and characterization of thin films. Many similar observations [3-10] were made as with the phosphors, such as green luminescence, but new observations were also made such as strong NBE emission. In fact, at low temperatures, a significant number of very fine and sharp peaks associated with bound excitons are usually present. There are various types of synthesis techniques that have been shown to create various nano sized morphologies. One of the earlier reports [6] of ZnO nanoparticles colloids shows a chemical reaction where Zn^+ and OH^- precipitated from an alcoholic solution. In recent years either a hydrothermal or sol-gel method became two of the most popular. The downside to these techniques is that unless the particles' surfaces are capped in a dielectric, the NBE emission will be significantly weaker than the defect emission. Since the particles created hydro thermally or through a sol-gel process must be dipped coated onto a substrate, a secondary process must then be used to do the capping. Various research groups [7] have also looked into the use of ion implantation for the creation of particles within a substrate. This is done by first implanting the substrate, usually SiO_2, with Zn ions and then a second time with O ions. After a subsequent annealing that varied from 300 to 700 °C, photoluminescence emissions near the band gap were found to be present. The growth process of the particles has been theorized to be a reverse Ostwald ripening. As the annealing temperature increases the intensity of the NBE emission increased.

One of the more important things to note is that even within the same synthesis procedure; there is a considerable variation in properties from batch to batch. There are a number of possible reasons for this, but usually the amount of oxygen in the environment is considered to be the culprit. Variations in other chemicals or impurities also play big roles. When it comes to the shapes of the particles, they can range from spherical, shells, rods, tetrahedrons, propellers, and many others. There have been reports that claim a link between the particle shape and spectra that is emitted, however looking across the literature as a whole, the connection between shape and properties appears to be unconvincing. Based on the wide variety of emissions seen within a given type of structures some other mechanism must be at work. Usually the NBE of as grown particles is rather weak and the defect emission, whether it is blue, green, yellow, orange, or red, is much stronger. One among the more interesting studies was from Shalish et al [8], who looked at nanorods of various sizes. They found that below a rod of radius 30 nm that the defect emission dominated the photoluminescence (PL) spectra, while above this size the NBE dominated. What they reasoned is that the defect emission is related to a recombination at the surface while the NBE emission is related to a recombination within the bulk of the material. This seems quite reasonable, since as the diameter of the rod becomes smaller, the ratio of the no. of atoms near the surface as compared to the bulk increases.

2.3 Basic Parameters

Zinc oxide (ZnO), an amorphous white or yellowish powder, has the molecular weight of 81.37, average atomic weight of 40.69 amu and an enthalpy of formation (298.15K) of 350.5 kJ/mol. Two main processes are employed for producing powdered zinc oxide. In the direct, or American, method of manufacture, zinc ores (or residues) are heated in air with coke or anthracite, and the resulting zinc vapour is subjected to controlled oxidation. In the indirect, or French, process, the zinc vapor to be oxidized is obtained by boiling zinc [9].

2.4 Structural, Electrical and Optical Properties of ZnO

ZnO normally forms in the hexagonal (Quartzite) crystal structure (6mm point group symmetry) with a=3.25 Å and c=5.12 Å. The Zn atoms are tetrahedral coordinated to four O atoms [6, 7] (Figure 2.1). The oxygen anions occupy the octahedral sites. The basic parameters of ZnO materials are presented in Table 2.1. As seen in Figure 2.2, the structure is non-centro symmetric, which gives rise to polarization and piezoelectric properties

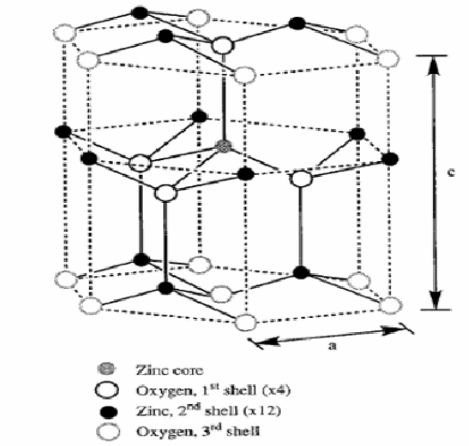

Figure 2.1: *Wurtzite (hexagonal) structure of ZnO [6, 7]*

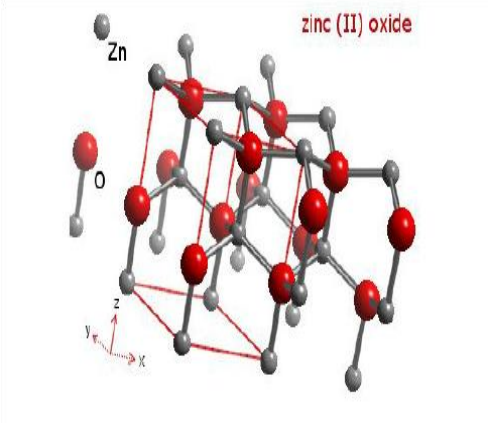

Figure 2.2: *Wurtzite (hexagonal) structure of ZnO*

Table 2.1: *Properties of Wurtize ZnO*

Property	Value
Lattice parameters at 300K	a_0 =0.32495 nm; c_0 = 0.52069 nm
Density	5.6803 g/cm^3
Melting point	1975°C
Thermal conductivity	100 mW/cm.K at 300K
Static dielectric constant	8.656
Refractive index	2.008
Energy gap	3.4 eV, direct
Intrinsic carrier concentration	< 10^6 cm^{-3} (max n-type> 10^{20}cm^{-3} electrons; max p type < 10^{17} cm^{-3} holes)
Exciton binding energy	60 meV
Electron effective mass	0.24
Electron Hall mobility at 330K	200 cm^2/Vs
Hole effective mass	0.59
Hole Hall mobility at 300K	5-50 cm^2/Vs

In the development of a crystalline morphology, the driving forces minimize the surface energy. Therefore, in near equilibrium conditions, a film grows with the crystallographic plane of the lowest free energy (i.e. the plane with the closest packing of atoms) parallel to the surface if no epitaxial exists between the film and substrate. ZnO tends to grow c axis oriented normal to the substrate with minimization of surface energy. ZnO is an II-

VI semiconductor which tends to intrinsically form as an n-type semiconductor material, in which the electrical conductivity is due to excess zinc, presumably interstitially within the lattice and in oxygen vacancies [9, 10]. Extrinsic defects such as hydrogen are more likely to be incorporated as shallow donors [10]. However, Studenkin et. al. [2] has reported that the effect of H incorporation increases the number of zinc rich defects and therefore n type conductivity. The defect chemistry for individually ionized Zn in vapor deposition can be written as follows [11]:

$$Zn(g) \rightarrow Zn_i \tag{2.1}$$

$$Zn_i \rightarrow Zn_i^{+} + e^{-} \tag{2.2}$$

$$Zn(g) + \tfrac{1}{2}O_2(g) \rightarrow ZnO(s) \tag{2.3}$$

Therefore, the overall concentration of interstitial ions is determined by the vapor pressure (usually high for Zn) as indicated in equation (2.1). The extent of interstitial ionization is also a dependent of temperature. The mass-action equation for (2.2) is:

$$K=[Zn_i^{+}][e^{-}]/P_{Zn}(g)=[e^{-}]^2/P_{Zn}(g) \tag{2.4}$$

$$[e^{-}]=K^{1/2} P_{Zn}(g)^{1/2}=K^{1/2} K_{0\,2} P_{O\,2}^{-1/2} \tag{2.5}$$

where KO_2 is the equilibrium constant for the reaction (2.3). It can be seen from equation (2.5) that the charge carrier concentration is a dependent of the partial pressure of oxygen. A general expression for electrical conductivity σ and the concentration of conduction electrons n and holes p in an intrinsic semiconductor is the following:

$$\sigma = n\, e\, \mu \tag{2.6}$$

$$n_i = p_i = A\, T^{3/2} \exp(-E_g/2\, k_B T) \tag{2.7}$$

where n_i or p_i is the number of conduction electrons or holes in unit volume, e is electronic charge, and μ is the mobility of current carriers, A is a constant, E_g is the energy gap, and k_B is the Boltzmann constant. Generally speaking there would appear to be five possible conduction mechanisms including: ionic conduction; space-charge-flow; tunneling and internal field emission; Schottky emission and impurity conduction [12]. There are few reports about the electrical conduction mechanism in ZnO. Hartmann et al [12] have showed that copper implantation of ZnO thin films deposited by sputtering decreases the resistivity, while oxygen annealing

increases the resistivity of the ZnO thin film due to electron trapping by the Cu 3d states of Cu^{2+}. It has been recognized that the presence of Al or Co has the effect of enhancing the electrical conductivity of ZnO thin films, whereas mono valent ions (Li, Na) usually hinder it [13]. The electron Hall mobility in ZnO single crystals is in the order of 200 cm^2/Vs at room temperature. Electron doping, in nominally undoped ZnO, has been attributed to Zn interstitials, oxygen vacancies or hydrogen. The optical properties of ZnO, such as photoluminescence, photoconductivity and absorption, reflect the fact that it has an intrinsic direct band gap, a strongly-bound exciton state, and gap states due to point defects [14]. A strong room temperature near band-edge UV photo luminescent peak at ~3.2 eV is attributed to an exciton state, as the excitation binding energy is of the order of 60 meV [8].

2.5 Applications of ZnO

ZnO is often used in the paint, paper, rubber, food and drug industries. It is also a promising material in nanotechnology applications, for example in nano-electronics and nano-robotic technology. With its wide band-gap, high exciton binding energy and high breakdown strength, ZnO can be utilized for electronic and photonic devices, as well as for high-frequency applications (Figure 2.3).

Figure 2.3: *Applications of ZnO*

To produce such optoelectronic devices, control of electronic properties, such as the nature of conduction and carrier density, is required. A few examples of applications of ZnO are discussed below.

2.5.1 Sensors

ZnO nanostructures are used for sensing applications because of their high sensitivity to the chemical environment. Nanostructures have the advantage of a high surface area, and electronic processes in them are strongly influenced by surface processes. ZnO nanowires have demonstrated high sensitivity even at room temperature, whereas thin-film gas sensors often need to be operated at elevated temperatures. The sensing process is governed by oxygen vacancies on the surface that influence the electronic properties of ZnO. Upon oxidation, via adsorption of molecules such as NO_2 at vacancy sites that accept electrons, electrons are withdrawn and effectively depleted from the conduction band, leading to a reduction of conductivity. On the other hand, reducing molecules such as those of H_2 can react with surface-adsorbed oxygen, leaving behind an electron and a higher conductivity. The challenge is to sense certain gases selectively. A ZnO nanorods H_2 sensor has been developed [12]. The sensitivity of this sensor was improved by sputter deposition of Pd clusters on the ZnO rod surface. The addition of Pd appears to be effective in the catalytic dissociation of H_2 into atomic hydrogen, increasing the sensitivity of the sensor device. The sensor detects hydrogen concentrations down to 10 ppm in N_2 at room temperature, whereas there is no response to O_2. By exposing the sensor to air or O_2, the conductance recovers up to 95% after 20 s. The same group has also shown H_2 sensitivity for Pt-coated ZnO nanorods [13].

Other workers used a thick film of ZnO nanoparticles for H_2 sensing [14]. A sensitivity of 10-1000 ppm H_2 was achieved for a Pt-impregnated, 3% Co-doped ZnO nanoparticles film at a working temperature of 125°C or lower. O_2, NO_2, and NH_3 oxidizing sensors in field - effect transistor geometry of single nanowires has also been demonstrated. The oxygen sensitivity is higher for smaller diameter nanowires and can be modulated by the gate voltage. Desorption of adsorbed NO_2 molecules is observed when a large negative gate voltage is applied. This can be used as a method to refresh the sensor to its original level. An ethanol sensor with good sensitivity and fast response at 300°C has been demonstrated using Pt inter dictating electrodes. Tetrapod-films prepared in a flow of humidified Ar show excellent performance in sensing ethanol with a short response time. A photocurrent gas sensor made of Ru-sensitized ZnO nano particles has been shown to be highly influenced by the gas molecules adsorbed on the surface. A CO molecule increases the number of electrons on the surface of ZnO and, therefore, leads to an increase in photoconductivity. On the contrary, O_2 can capture electrons directly on the surface and lower the concentration of charge carriers in the ZnO conduction band and, therefore, the photoconductivity. A glucose sensor based on ZnO nanorods has also been reported. The negatively charged glucose oxidase (GOx) enzyme is immobilized on positively charged ZnO through electrostatic forces. At an applied potential of +0.8 V versus an Ag/AgCl reference electrode, the glucose biosensor shows a linear response from 0.01-3.45 mM and an experiment limit of detection of 0.01 mM. The response time has been found to be less than 5 s.

2.5.2 Light-emitting diodes and lasing

Bao et al [14] have constructed a single nano wire light-emitting diode. They disperse ZnO nano wires on a Si substrate and then a poly (methyl methacrylate), or PMMA, thin film is spin-coated onto the substrate. The wire is imaged in a focus ion beam (FIB) system and a pattern for e-beam exposure of the PMMA is defined. The unexposed and partially exposed PMMA is removed and then a metallic contact is deposited onto the top surface of a single nano wire. In this way, the researchers were able to measure the current-voltage characteristics, photoluminescence, and electroluminescence of a single nano wire.

2.5.3 Cantilevers

Lee et al [15] have proposed the use of well-aligned single-crystalline nano wires as sharp atomic force microscopy (AFM) tips. They predict that ZnO nano wires are structurally compatible with AFM cantilevers under typical conditions and are promising candidates for high-aspect-ratio probes for AFM. Huang et al [16] have characterized the mechanical resonances of a single nano wire using an alternating electric field. They have monitored the flexural mode of the nano wire in situ in a transmission electron microscope (TEM). With an elastic bending modulus of ~58 GPa and a damping time constant of ~14 ms for the resonance in vacuum, the authors conclude that a single ZnO nano wire can be used as a nano resonator and a nanoscale cantilever.

2.5.4 Solar cell

ZnO has also been used in dye-sensitized solar cells as an electrode material [17-20]. Investigations of nano porous dye-sensitized ZnO films have shown that ultrafast electron injection from the dye into the conduction band of the ZnO particles takes place [21-24] at a time scale comparable to that of electron injection into TiO2 layers; which has been the subject of investigation for a long time [25]. Semiconductors should have a wide band gap, high charge carrier mobility, and films fabricated from the material need to deliver a high surface area for efficient dye-sensitization and light harvesting, which can only be achieved by a nanostructure film. Therefore, ZnO seems to be a promising material for this type of solar cell and has the advantage over other metal oxides of easy synthesis of controlled nanostructures. Dye-sensitized solar cells usually have an electrolyte (redox system) to regenerate the dye by electron donation to its Ground state after action.

2.6 Current Developments in ZnO

2.6.1 n and p Type ZnO

For ZnO, n-type conductivity is common in the as grown material, or relatively easy to realize via excess Zn, or with Al, Ga, or In doping. Reports indicate that the resistivity of ZnO or Al doped ZnO thin films prepared by magnetron sputtering are in the range of 10^{-4} to 10^{-5} Ω cm [30, 31]. A common opinion is that Zn–rich defects such as zinc interstitials (Zn_i) and oxygen vacancies (V_O) are the main source of conductivity in as grown material. Thus, the conductivity of films can be determined by the degree of non-stoichiometry of ZnO. It has been found that many factors affect the electrical properties of ZnO thin films such as film thickness, grain and agglomerate size, grain boundary and impurity distribution, all of these are determined by the synthesis conditions. However, the effect of microstructure on the electrical properties of ZnO thin films and related

correlations has not been widely discussed in the literature. Without question, the most significant barrier to the widespread exploitation of ZnO related materials in electronic and photonic applications is the difficulty in carrier doping, particularly as it relates to achieve p-type material. With respect to p-type doping, ZnO displays significant resistance to the formation of shallow acceptor levels. The shallow level is shown in Figure 2.4, the band model of ZnO [32, 33]. The model consists of conduction band and valance band. The energy difference between them is the energy gap of ZnO, ~ 3.37 eV. The Fermi energy is the maximum energy level occupied by an electron at 0K.

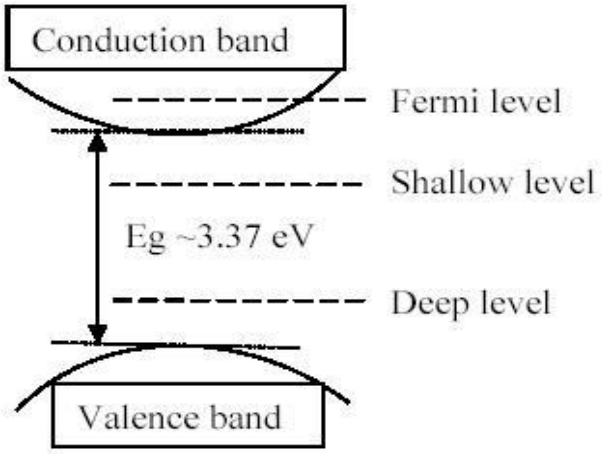

Figure 2.4: *The band model of ZnO*

2.6.2 ZnO and Nanotechnology

Nanoscience and nanotechnology involve studying and working with matter on an ultra-small scale from sub nanometer to several hundred nanometers [48]. These nano size materials have properties that are often significantly different from their counterparts with "ordinary size". Nanotechnology is the next phase of Moore's Law. This law was predicted in 1965 that the dimension of a device would halve approximately every 18 months. By combining silicon innovations with other novel non-Si nanotechnologies, it is expected that Moore's Law will extend well into the next decade [49]. ZnO is a promising material for the realization and future of nanotechnology. With its wide band-gap (3.37eV), high excitonic binding energy and high breakdown strength, ZnO can be utilized for electronic and photonic devices, as well as for high-frequency applications. The availability of a native substrate and the potential for room temperature operations opens the door to ZnO applications including chemical sensors and subscale electronic circuits. As a source of unique properties, Zinc Oxide (ZnO) has been widely studied as a novel material for its practical and potential applications such as micro, nano-electronics and micro, nano-robotic (machining) technology [50]. Several synthesis methods of ZnO nanoparticles or nanocrystalline films, such as sputtering, pulsed laser deposition, epitaxial techniques and chemical routes have been developed. Mechanical attrition also appears to be a suitable method for obtaining semiconductor nanocrystals [51].

Recently, the preparation of basic one-dimensional nanostructures and their assembly in two-dimensional and three-dimensional ordered architectures have been a major challenge faced by the modern synthetic chemists and materials scientists [52]. Up to now, much effort has been devoted to the fabrication of well-defined ZnO 1D nanostructure such as nanowires (or nanorods) [53], nano belts nanoribbons [54], nanorings [55], nanocolumns [56], nanonails [57] and well-aligned ZnO nanorods and nanotubes arrays [58]. One-dimensional ZnO nanostructures such as nanowires and nanorods have been studied for optoelectronic nanodevice applications as a promising candidate for UV light-emitting diodes and laser diodes because of both their fundamental importance and the wide range of their potential applications in nanodevices. ZnO nano-wires have potential for applications in laser devices due to their desirable optical properties. Therefore, a detailed understanding of ZnO wires and the influence of impurities on their properties is important. ZnO nanorods can be grown or deposited on various substrates including Si [59]. Many groups have recently demonstrated the catalyst-driven growth of ZnO nanorods using MBE or vapor transport [60, 61]. The large surface area of nanorods makes them attractive for gas and chemical sensing, and the ability to control their nucleation sites makes them good candidates for micro-lasers or memory arrays. Nanorods and nano-wires will lead to the possibility of nano devices, such as nano-lasers or memory arrays [62]. A SEM micrograph of a single rod is shown in Figure 2.5 (a). In addition, ZnO nano-particles are equally interesting and can be grown and synthesized by different methods. These nano-particles are of great interest since they have many technological as well as medical applications.

Exchange-spring magnets are nano composites that are composed of magnetically hard and soft phases that interact by magnetic exchange coupling. Such systems are promising for advanced permanent magnetic applications [63]. The two-dimensional system of thin coatings has been studied widely. Three dimensional (3D) interconnected networks of ZnO nanowires and nanorods are synthesized by a high temperature solid–vapor deposition process [64]. The nanorods and nanowires have diameters of 20–100 nm and they grow along the c-axis. The thickness of the multilayer nano-network could be as thick as 30 μm. The sharp nanowires tips, the high degree of networking, and the high surface area of these unique nano networks make them a potential candidate for field emission, ultra-sensitive gas sensing, catalysts and filtering. Large-scale synthesis of ZnO nanowires has been achieved on Au-coated silicon substrates by physical evaporation of the mixture of ZnO, graphite powders and polycrystalline ZnO nanowires have been fabricated within the nano channels of porous alumina [65].

More recently, complex and oriented ZnO 3D structures, e.g. flower- and urchin-like assemblies [58], dandelion-like structures [66], hollow microspheres [67], polyhedral cages and shells [68], complex architecture [69], and hierarchical nanostructure [70], comb-like nanowire arrays, nanoneedle arrays [71], nanohelics (Figure 2.5 (b) [72]), and nanobows [73] have been successfully synthesized. For example, single crystalline ZnO nanohelices have been prepared by thermal evaporation of ZnO powder. The piezoelectric and semiconducting properties of ZnO suggest that the nanohelix could be a fundamental unit for investigating electromechanically coupled nanodevices by using the super lattice piezoelectric domains. The nanohelix is likely to have important applications in sensors, transducers, resonators, and photonics. The structural configurations of ZnO nano-objects could form the basis for fabricating nanoscale sensors, transducers, and resonators [72]. In this study

nano-ZnO and polymer composites have been made in a water solution. This is a novel method of producing these materials.

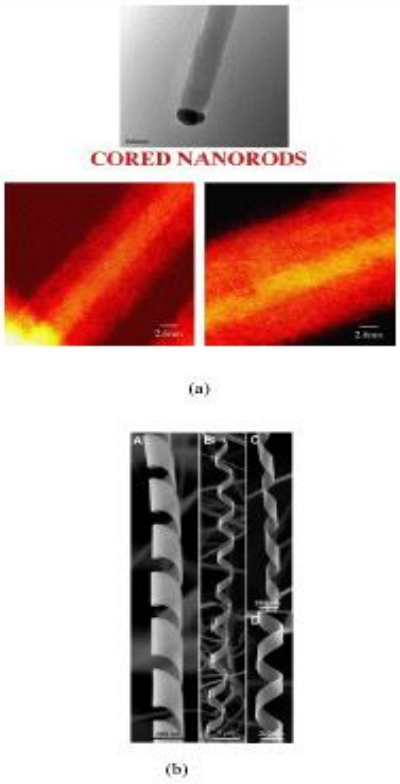

Figure 2.5: *(a) TEM images of single-crystal ZnO nanorod (top) and showing cored (Zn1-xMgx) O nanorods (bottom) (b) SEM images of the left- and right-handed ZnO nanohelices [72]*

2.6.3 Implantation Doping

Ion implantation is an important and controllable technique of introducing dopants into a semiconductor and creating high resistance regions for inter-device isolation. Dopants may become embedded in the solid and may occupy the interstitial positions, there by changing the chemical composition of the solid. Implantation doping is in its infancy in ZnO and there has been no clear demonstration of activation of an implanted donor or acceptor. Damage due to ion implantation may occur as a result of ionization as well displacement collisions, associated with diffusion processes and phase changes. The residual implantation damage remaining after annealing appears to have donor-like characteristics. To minimize this damage, it may be necessary to adopt techniques used for other compound semiconductors, such as elevated temperatures during the implantation step, to take advantage of so-called dynamic annealing in which vacancies and interstitials created by the nuclear stopping process are annihilated, before they can form stable complexes [72]. Ion implantation is used for introducing conduction carriers and optical isolation, dry etching, and ion slicing. A wide range of implant

conditions (implanted species, ion mass, dose ($10^{12\text{-}18}$ atoms cm^{-2}), and implant temperature) affects the formation of lattice interstitials, vacancies and planar defects in a crystal such as GaN and ZnO [74]. Ion implantation of potential p-type dopants and co-implantation studies are beginning to show promising results for producing p-type ZnO [75]. Miyakawa [76], Komatsu [36], Jeong [77] and Ip [78] have reported implantations of As, In, N, Ga and H in a ZnO crystal at room temperature. Hartmann and Puchert [27] reported Cu implantation of ZnO thin films. Kucheyev et al [79] have recently reported a systematic study of implant isolation in n-type ZnO epilayers grown on sapphire. Mn-implanted (5×10^{16} atoms cm^{-2}) ZnO nanorods samples show magnetization vs. magnetic field (H) behaviour at 300 K after a 700 °C, 5 min anneal (Figure 2.6). Hysteretic behaviour is clearly present. Possible explanations include ferromagnetism, super paramagnetism or spin-glass effects. The magnetization of Mn implanted, annealed nanorods was as much as 3 orders of magnitude lower than in the implanted, annealed samples, demonstrating that the transition metals are responsible for the observed magnetic properties [72].

There was no significant chemical effect noted for Cr, Fe or Ni implantation relative to O, indicating these elements do not introduce a large concentration of deep acceptors into ZnO.

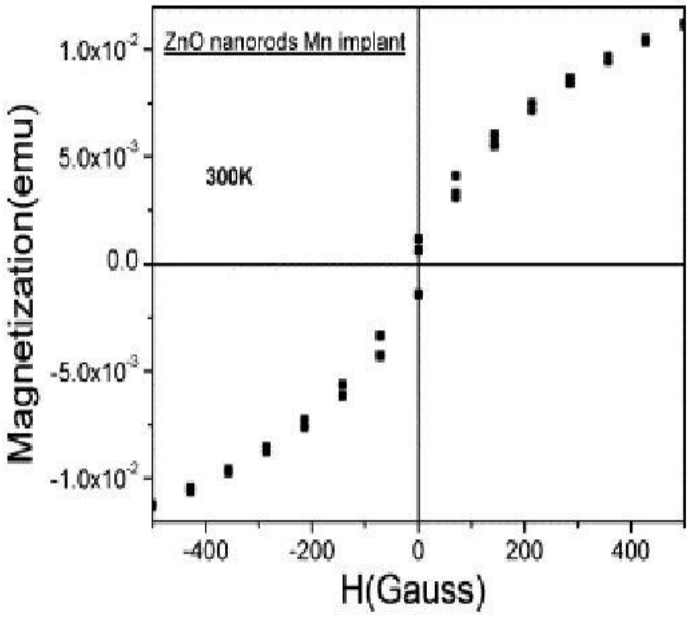

Figure 2.6: Magnetizations vs. field at 300 K for Mn-implanted ZnO nanorods [72]

In transparent oxides, although the implantation is mainly applied to the fabrication of optical devices such as wave guides and fluorescent materials, the history of application to carrier control is rather new as an approach to the fabrication of p-type ZnO. In this study, the dopants, Al, Ag, Sn, Sb, and TiN, are selected for this investigation to determine if these species can improve the conductivity of ZnO thin films and impart p-type properties to ZnO.

2.7 Composites and ZnO

A composite material consists of a combination of materials which differ in composition or form, remain bonded together, and retain their identities and properties. Composites include: (1) fibrous (composed of fibres, and usually in a matrix), (2) laminar (layers of materials), (3) particulate (composed of particles or flakes, usually in a matrix), and (4) hybrid (combinations of any of the above) [80]. Laminar and particulate composites have been used in the ZnO composites such as ZnO thin films deposited on PEN, nano- ZnO particles and polyvinyl alcohol blends and Al, Ag, Sn, Sb and TiN implanted ZnO thin films. The ancient concept of composite materials was to combine different materials to produce a new material with performance unattainable by the individual constituents, e.g. adding straw to mud for building stronger mud walls. More recent examples are carbon black in rubber and fibre glass in resin etc. Epoxy resin composites are filled with nano-particulates using a KH-560 silence coupling agent to enhance the interfacial bonding between the inorganic reinforcing agent and the polymer matrix [81]. The incorporation of modifying Zn ions into "poly diene latex-silica" systems increases their mechanical characteristics due to an increase of the interaction between the organic and inorganic networks [82]. In nature, examples are a bound: cellulose fibres in lignin matrix (wood), collagen fibers in an appetite matrix (bone) etc. Today, given the most efficient design, of for example an aerospace structure, a boat or a motor, we can make a composite material that meets or exceeds the performance requirements because of its unique combination of properties. Most of the savings are in weight and cost. These are measured in terms of ratios such as stiffness/weight, strength/weight, etc. [83, 84].

2.7.1 Advanced Processing Methods

There are many deposition techniques for ZnO thin films. Thin film deposition technologies can be either purely physical, such as evaporative methods, or purely chemical, such as gas and liquid phase chemical processes. A considerable number of processes (that are based on glow discharges and reactive sputtering) however combine both physical and chemical reactions and can be categorized as physic-chemical methods. Thin films of ZnO can be grown by-

(a) Sol gel processing,
(b) Molecular beam epitaxial,
(c) Chemical vapor deposition,
(d) Magnetron sputtering,
(e) Pulsed laser deposition, and
(f) Spray pyrolysis on several different substrates [27, 28].

2.8 Zinc Oxide Synthesis Techniques

ZnO nanostructures are usually obtained via a vapor transport process. Depending on the synthesis condition variations in temperature, catalyst, and composition of source materials, a wide range of nanostructures has been obtained. Using a vapor-solid process, complex ZnO nanostructures such as nanohelixes, nanorings and nanobelts were synthesized by Kong et al In this process, ZnO powder was decomposed into Zn2+ and 0 2- at 1400 ^{0}C then transported by Ar carrier gas to a low temperature zone (400 ^{0}C), and nanostructures were

formed on a collecting chip. In a similar vapor transport and condensation process reported by Ren et al [57], hierarchical ZnO nanostructures were grown by mixing ZnO, In_2O_3 and graphite powder and heated up to 820-870 ^{O}C. A simplified method to achieve nanowires, nanoribbons and nanorods was reported by Yao et al [18, 31] ZnO powder was mixed with graphite and heated to 1100^{O}C then cooled down, nanostructures were found to form on the wall of the furnace. These synthesis methods utilize the vapor-solid (VS) mechanism, in which ZnO nanostructures are formed by condensing directly from vapor phase. Although diverse nanostructures can be obtained, this method provides less control on the geometry of ZnO nanostructures. Controlled growth of ZnO nanowires has been achieved by using various nanoparticles or nanoclusters as catalysts, such as Au. In these cases, ZnO and carbon powder are usually used as source material and a vapor-liquid-solid (VLS) growth mechanism governs the synthesis. In the VLS mechanism, the catalyst nanoparticles become liquid droplet under reaction temperature. The reactant Zn vapor generated by carbon thermal reduction of ZnO powder is transported to the catalyst nano-droplets and form Zn-catalyst alloy. In the meantime, ZnO forms as a result of the reaction between Zn and CO/CO_2. Upon supper saturation, ZnO nanowires grow from the droplets. Recently we have found that this synthesis process can be further simplified by directly heating pure Zn powder in low concentration oxygen environment (2%) using Au nanoparticles as catalysts.

A variety of methods exist for ZnO deposition and growth. For consolidation, methods have been categorized as either physical vapor deposition (PVD), chemical vapor deposition (CVD), or solution-based chemistry (SBC). Each respective method can be subdivided into the individual techniques that are summarized in Table 2.2 below [85]

Table 2.2: *Methodologies for ZnO deposition and growth*

Physical Vapor Deposition (PVD)	Thermal evaporation *Electron-beam* *RF induction* *Resistive* Sputtering *Focused ion beam* *Radio frequency* *Magnetron* Pulsed Laser Deposition
Chemical Vapor Deposition (CVD)	Thermal CVD Low pressure CVD (LPCVD) Plasma enhanced CVD (PECVD) Metal-organic CVD (MOCVD) Molecular beam epitaxy (MBE) Atomic layer deposition (ALD)
Solution-based Chemistry (SBC)	Hydrothermal Sol-gel

2.8.1 Physical Vapor Deposition

Physical vapor deposition (PVD) occurs when a material is physically released from a source and transferred to a substrate. The three most important technologies for ZnO deposition are thermal evaporation, sputtering, and pulsed laser deposition; each of which will be described below.

2.8.1.1 Thermal Evaporation

During thermal evaporation, the substrate, crucible, and source material are placed inside a vacuum chamber at room temperature. A vacuum is required to increase the vapor pressure during sublimation and often ranges between 10^{-2} & 10^{-9} Torr (ultra-high vacuum). Once the vacuum chamber has stabilized at the appropriate pressure, a heating source is used to heat the source material within the crucible to its vapor point. Upon evaporation, the material will re-deposit along the cooler surfaces of the vacuum chambers, as well as the collection substrate. Typical heating sources include electron-beam, radio-frequency (RF) inductive, and resistive heating. During electron-beam evaporation, an electron source is aimed at the source material causing localized heating. In comparison, RF induction uses an AC power supply to produce an alternating current through an induction coil. The alternating current generates a magnetic field within the coil. When the source material is placed inside the coil, the magnetic field induces eddy currents within the source material providing localized heat. Although higher frequencies equate to higher heat rates, lower frequencies are better suited for thicker samples. Finally, resistive heating provides heat by sending a high current source through a resistive coil, such as tungsten, and is a non-localized heat source and therefore commonly used for furnace applications. Although inductive RF and electron-beam sources have been limited to highly-oriented, thin-films of ZnO [86] resistive sources have produced thin-films, as well as a diversity of ZnO nanostructures with different shapes, sizes, and orientations [87, 88].

2.8.1.2 Sputtering

Sputtering is the removal of surface atoms via high energy ions. Sputtered films are typically polycrystalline and form at low temperatures with good adhesion properties. Common types of sputtering are focused ion-beam, direct current (DC), radio-frequency (RF), and magnetron. During focused ion-beam sputtering, gallium ions are accelerated through a vacuum towards a sample surface. Acceleration and focusing capabilities are provided by a series of capacitive plates and magnetic coils, respectively. In general, the focused beam of ions provides an exquisite tool for milling and cutting at the nanoscale and has been used within this work as a tool for building prototype nanobelts devices. In comparison, during DC sputtering, the substrate and source (target) material are placed inside a vacuum chamber. Upon evacuation of foreign gases, an inert gas, such as argon, is introduced into the chamber at low pressures. Then, a DC power supply is used to ionize the inert gas in order to produce charged plasma. The ions are accelerated towards the surface of the target, causing atoms of the source material to break off from the target and condense on all surfaces including the substrate.
A limitation to DC sputtering is the high voltage required to sputter insulating materials due to the build-up of positive charge on the target material. To solve this problem, the DC power source should be replaced by an RF power source (RF sputtering). In addition, a strong magnetic field (magnetron sputtering) can be used to

concentrate the plasma near the target to increase the deposition rate. When applied to ZnO, sputtering has been limited to polycrystalline thin-films [89].

2.8.1.3 Pulsed Laser Deposition

During pulsed laser deposition (PLD), a laser beam is focused through a vacuum onto the surface of a target material. At sufficiently high flux densities and short pulse durations, the target material is rapidly heated to its evaporation temperature and forms a vapor plume. Unlike thermal evaporation, where the vapor composition is dependent on the vapor pressures of the elements within the source material, laser ablation produces a plume of material with similar stoichiometry to that of the target material. Once the vapor plume has been formed, it is collected onto a cooler substrate that promotes nucleation and growth of crystalline films. It is important to note that by using a single crystal substrate; epitaxial single-crystals can be grown that are equal in quality to molecular beam epitaxy. As applied to ZnO, fabrication of (0001) epitaxial films on cubic (111) substrates have been formed using pulsed laser deposition [90] as well as aligned ZnO nanorod [91, 92] and nanodot [93] arrays without the aid of a catalyst.

2.8.2 Chemical Vapor Deposition

During chemical vapor deposition (CVD), the substrate is placed inside a reaction vessel where the pressure and gas flow are controlled. Fundamentally, the process is a chemical reaction between source gases; the product of which condenses during the formation of a solid material within the reaction vessel. The most common CVD techniques used to deposit ZnO are thermal CVD, low pressure CVD (LPCVD), plasma-enhanced CVD (PECVD), metal-organic CVD (MOCVD), molecular beam epitaxy (MBE), and atomic layer deposition (ALD). For each of these methodologies, a vacuum chamber with gas flow control is required.

2.8.3 Solution-Based Chemistry

Solution-based chemistry (SBC) is the study of any chemical reaction that requires a liquid. As a generic method for synthesis, SBC has been vital to the production of a diversity of materials that are often difficult to make using PVD or CVD. Typically, solution-based methodologies provide materials with high yield and uniformity. However, a common drawback is an increased number of points, line, and planar defects when compared to their simpler physical counterparts. The most important and common techniques for ZnO synthesis are hydrothermal and sol-gel synthesis, both of which will be discussed below.

2.8.3.1 Hydrothermal Synthesis

As defined, hydrothermal synthesis is a subset of solvothermal synthesis which involves water at elevated conditions. The basic principle is that small crystals will homogeneously nucleate and grow from solution, when subjected to high temperatures and pressures. During the nucleation and growth process, water is both a catalyst and occasionally a solid-state phase component. Under the extreme conditions of the synthesis vessel (autoclave or bomb), water often becomes supercritical, thereby increasing the dissolving power, diffusivity, and mass transport of the liquid by reducing its viscosity. In addition, the ability to tune the pressure of the vessel provides an avenue to tailor the density of the final product. When compared to other methodologies, hydrothermal

synthesis is environmentally benign, inexpensive, and allows for the reduction of free energies for various equilibrium. Materials that are made hydrothermally are generally high-quality, single crystals with a diversity of shapes and sizes. Although hydrothermal synthesis is an established synthesis route within the ceramics industry, it has recently been rekindled within the scientific community by synthesizing one-dimensional nanostructures, such as carbon nanotubes and oxide nanowires. As of recent, hydrothermal synthesis has been used to synthesize well-aligned ZnO nanorods on GaN substrates for optical applications [106].

2.8.3.2 Sol-Gel Synthesis

The sol-gel process, as the name implies, involves the evolution of inorganic networks through the formation of a colloidal suspension (sol) and gelation of the sol to form a network in a continuous liquid phase (gel). The precursors for synthesizing these colloids consist of a metal/metalloid surrounded by various reactive ligands. Metal alkoxides are most popular because they react readily with water. At the functional group level, three reactions are generally used to describe the sol-gel process: hydrolysis, alcohol condensation, and water condensation. However, the characteristics and properties of a particular sol-gel inorganic network are related to a number of factors that affect the rate of hydrolysis and condensation reactions, such as pH, temperature and time of reaction, reagent concentrations, catalyst nature and concentration, aging temperature and time, and drying. When applied to ZnO, nanocrystals [107] thin films [108] and nanorods [109] have been synthesized with preferred crystallographic orientations using the sol-gel method. The synthesis of ZnO nanostructures, fabrication and electrical characterization of ZnO nanobelt devices, and predictive modeling intended to guide future research.

2.9 Growth Mechanism

Crystal solidification occurs by one of two means. Either a vapor condenses into a liquid which then condenses into a solid, or the vapor bypasses the liquid state and transforms directly to the solid state. Primary barriers to solidification are heterogeneous nucleation and growth which can be reduced using precise control of the synthesis conditions. Among one-dimensional nanostructures, two mechanisms are used to explain nucleation and growth during physical vapor deposition. The first mechanism is vapor-solid (VS) growth and the second is vapor-liquid-solid (VLS) growth. However, for the thrust of this research, vapor-solid growth was used and therefore will be the only mechanism discussed below.

2.9.1 Vapor-Solid Growth

Vapor-solid growth of one-dimensional nanostructures is historically based on whisker formation. As defined, a whisker is a single-crystalline eruption from the surface of a deposited metal film. Typically, whiskers are 5 microns in diameter with lengths between 1 and 500 microns. The first observation of a whisker was made in 1946 by H.L. Cobb [113] during the evaluation of electrical component failure caused by the formation of cadmium whiskers. This work was independently confirmed by K.G. Compton et al [114] of Bell Laboratories in 1951 when observing similar phenomenon in electroplated cadmium (Cd), zinc (Zn), and tin (Sn), as well as growth in an aluminum (Al) casting alloy and on electroplated silver (Ag) exposed to hydrogen sulfide (H2S). Within this work, the authors speculated without conclusion that the whiskers are “not compounds but are

metallic filaments in the form of single crystals." In 1952, Herring and Galt inferred that whiskers were single-crystals because of their mechanical properties [115]. Then in 1953, the first dislocation theory for whisker growth was proposed by Peach [116]. Within this theory, the terminal step of a screw dislocation provides an energy sink to promote physical deposition where the Burgers' vector is parallel to the whisker's growth direction. However, this theory was quickly overshadowed in 1954 when Koonce and Arnold of Bell Laboratories published their seminal work describing that whisker growth occurred by the continual addition of material to the base of a whisker rather than by addition of material to the tip of the whisker [117]. Resounding evidence was provided by a series of electron micrographs, taken over several weeks, showing that the whisker tip shape did not change over time even though the overall length of the whisker increased. To date, this observation is consistent with current findings. Although F.C. Frank [118] and J.D. Eshelby [119] in 1953, and then S. Amelinchx et al [120] in 1957, proposed dislocation theories describing root growth of whiskers, the lack of microscopy evidence confirming the existence of dislocations eventually lead to the abandonment of all dislocation theories [119]. In 1955, Sears [121] proposed that for sufficiently small vapor super saturation, growth could occur at the tip of the whisker rather than at its base. Within this model, atoms simultaneously condense at the tip, as well as the sidewalls of the whisker. Under the assumption that nucleation and growth only occur at the growth front, condensed atoms must either migrate to the tip of the whisker or absorb from its surface.

2.9.2 Whisker growth characterization

As a diffusion-limited growth process, Sears suggested that whisker growth was exponential when the whisker length was less than the mean migratory distance of the adsorbed atoms. In comparison, if the length of the whisker was greater than this mean distance, the growth rate would become linear since the atoms would arrive at the tip at a constant rate with dependency on the partial pressure of vapor within the atmosphere. More specifically, if h is the instantaneous length at time, t, and h_0 is the length at t = 0, then the exponential growth is given by:

$$h=h_0 \exp(not/g) \qquad 2.8$$

where *n* is the number of atoms condensing onto the surface per unit area per second and g is a geometrical constant [122] Expanding on Sears' concept, Blakely and Jackson [122] in 1962 solved for the two-dimensional nucleation probability (P_n) on the surface of a whisker:

$$pn = B \exp [-\pi\sigma^2/k^2T^2ab \ln\alpha] \qquad 2.9$$

where B is a constant, σ is the energy of the solid nanowire, k is the Boltzmann constant, Tab is absolute temperature and α is defined as a ratio between the actual vapor pressure p,and the equilibiruim vapor pressure p0 at temperature Tab (α=p/po) upon evaluation of Equation 2.9, lower surface energies correspond to greater two-dimensional nucleation probability. However, low energy surfaces also have smaller sticking coefficients when compared to their higher energy counterparts. As a consequence, adsorbed atoms will have a higher probability of desorption on these low index surfaces. Balance between these two distinct effects is fundamental to the formation of the low-index crystal planes that commonly enclose whiskers and one-dimensional

nanostructures. As a consequence of this research, whiskers, as well as one-dimensional nanostructures, are thought to be kinetically-driven, anisotropic, crystallization processes that are heavily dependent on super saturation [123]. Fortunately, the temperature and super saturation ratio are easily controlled parameters during synthesis. Higher temperature and larger super saturation ratios facilitate two-dimensional nucleation resulting in the formation of films. In comparison, lower temperatures and smaller super saturation ratios are preferred for the nucleation and growth of wire-like structures. To sum up, temperature and the 'super saturation ratio' are the two dominant factors relevant to VS growth.

2.9.3 Self-Catalysis

Although, qualitative intuitive understanding, more research is required to develop a predictive model for one-dimensional nanostructures. Based on the aforementioned criteria, the VS growth process can be considered 'self-catalyzed'. As applied to ZnO, Dai et al [124] have developed a conceptual model to explain the VS growth of ZnO nanobelts. It is schematically shown in Figure 2.7, ZnO vapor molecules are released from the solid state at elevated temperatures and they then condense onto a substrate located in a cooler region of the furnace (Figure 2.7(A)). Upon arrival of additional molecules, a critical nucleus will develop (Figure 2.7(B)) and it will continue to grow with each adsorbed molecule (Figure 2.7(C)). Throughout this process, the local vapor super saturation remains constant, through pressure control within the furnace. As a consequence of the relatively high mobility of the molecules at the deposition temperature (~800ºC), molecules migrate to the high-energy growth front, in a series of steps (Figure 2.7(D)). The rough tip surface becomes an 'energy sink' for incoming vapor molecules resulting in the rapid formation of a 'nanobelts' (Figure 2.7(E)).

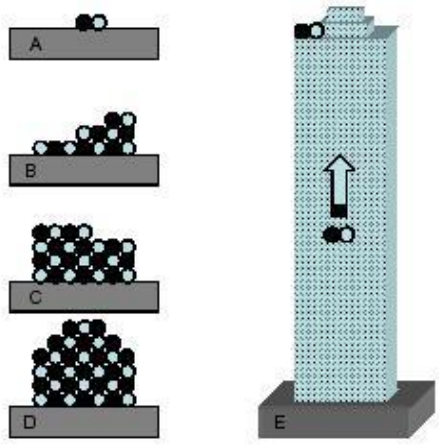

Figure 2.7: *A proposed growth mechanism for ZnO nanobelts through a VS process [124]*

Confirmation of the model depicted in Figure 2.7 is shown below in Figure 2.8, where the growth front of an individual ZnO nanobelt is rounded. The rounded surface indicates atomic-scale roughness through the presence of steps, ledges, and kinks. This high energy surface readily adsorbs ZnO vapor molecules and leads to the anisotropic growth of ZnO nanobelts. It is important to note that the TEM micrograph below is obtained in the absence of a catalyst and therefore the ZnO nanobelt is believed to be self-catalyzed.

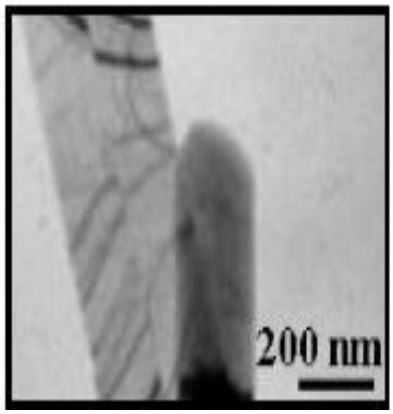

Figure 2.8: *A transmission electron microscopy image showing the growth front of a ZnO nanobelt*

2.9.4 Conductivity

Magnetron sputtering is a popular technique to prepare thin films (Figure 2.9). Zinc oxide thin films were prepared by dc (direct current) and rf (radio frequency) magnetron sputtering on glass substrates. The reported resistivity of ZnO or Al doped ZnO thin films prepared by magnetron sputtering are in the range of 10^{-4} to 10^{5} cm [125,126]. Generally, Zn– rich defects such as zinc interstitials (Zn_i) and oxygen vacancies (V_O) are believed to be the main source of conductivity in as grown ZnO samples [127,128]. The effects of several parameters like film thickness, grain and agglomerate size, grain boundaries and impurities on the electrical properties of ZnO thin films have been reported [129-132]. However, there are fewer reports addressing the relationships of microstructure on the optical and electrical properties of ZnO thin films. It has been found that ZnO films produced by dc sputtering have a high resistance, while the films produced using rf sputtering are significantly more conductive. While the conductive films have a compact nodular surface morphology, the resistive films have a relatively porous surface with columnar structures in cross section. Compared to the dc sputtered films, rf sputtered films have a microstructure with smaller d-spacing, lower internal tress, larger band gap energy and higher density.

The dependence of conductivity on the deposition technique and the resulting d-spacing, stress, density, band gap, film thickness and Al doping are discussed. Correlations between the electrical conductivity, micro structural parameters and optical properties of the films have been made. However, the relationship between the band gap and the conductivity of ZnO thin films is complex. A series of ZnO films were deposited by dc and rf magnetron sputtering using direct and reactive sputtering modes. Argon or argon-oxygen mixtures were used as the plasma-forming gas. Working pressure in the chamber was varied from 2 to 20 m Torr keeping the cathode-to-substrate distance 13 cm and deposition time 1-4 hrs. The sputtering targets were ZnO (99.9%) or Zn (99.99%), with an Al thin strip attached on the surface of the target for Al doping. Microscopic glass slides were used as substrates, which were in rotation during deposition. The principle of sputter deposition of ZnO thin films is shown in Figure 2.10. To initiate the process, a large negative potential is applied between target and the ground so that electrons are emitted from the target surface. The ejected electrons accelerate through

the potential. They collide with gas atoms and ionize them. Positive ions are accelerated to the cathode. When they hit the target, different types of particles are emitted. There are of course neutral atoms that will eventually get to the substrate and build the film, but also negative ions, photons and secondary electrons. If the secondary electron yield is high enough, plasma will be created. ZnO thin films were deposited under various deposition conditions. The electrical resistivity of the films was measured by standard two-probe and four probe (Figure 2.11) techniques. Scanning electron microscopy (SEM, Philips XL-30S with Energy-dispersive X-ray (EDX) using analytical ZnO pellets as standard materials) and X-ray diffractometer (XRD, Bruker D8, Cu Ka) were used to characterize the microstructure of the films. SEM was used for thickness measurement of the films. Hall coefficients of the samples were measured at room temperature by an automated dc Hall measurement system using the technique devised by Van Der Pauw in the laboratory of National University of Singapore. A HP 8254 spectrophotometer was used for recording the optical transmission spectra of the samples in the 190 – 800 nm spectral range.

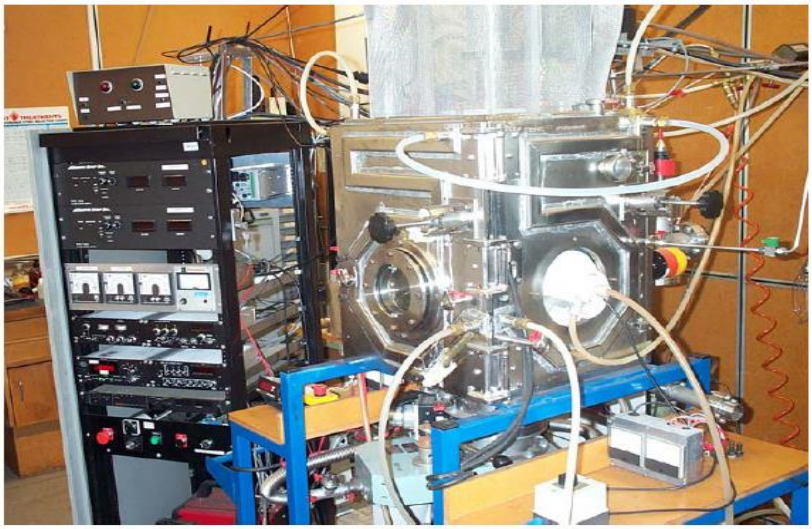

Figure 2.9: *Magnetron sputtering*

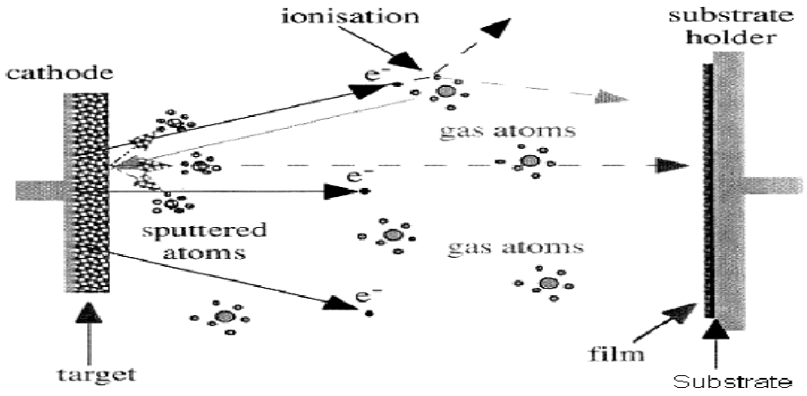

Figure 2.10: *Magnetron sputtering deposition principles*

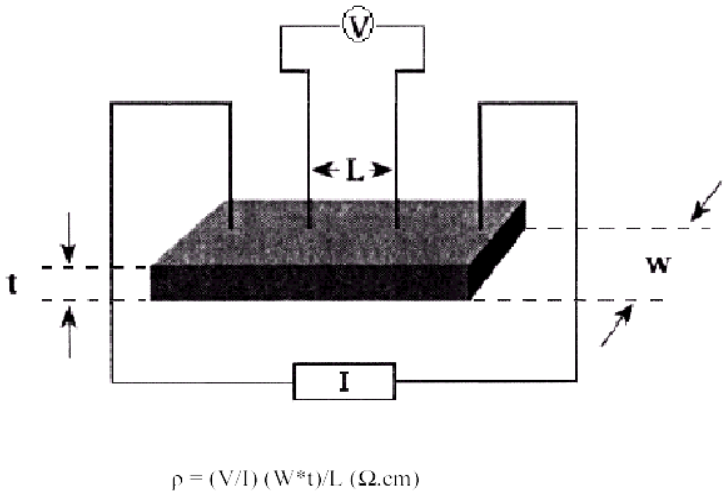

Figure 2.11: *Four-probe technique for measuring conductivity*

The XRD patterns of the ZnO films are shown in Figure 2.12. The patterns revealed only strong (002) and weak (004) peaks, indicating a strong preferred orientation perpendicular to the substrate. As the surface energy density of the (002) orientation is the lowest in a ZnO crystal, (002) orientation is favoured in the film [133]. In most of the samples, d002 values are higher than the standard d002 value for unstressed powder (0.26033 nm, ASTM [134] suggesting an elongation of unit cells along the c axis, and existence of compressive stresses along the plane of the films. From diffract ion simulations using 'Rietan 2000' (Authors: F. Izumi and T. Ikeda), if strong preferred orientation to the C-axis is introduced into the calculation, only (00n) diffraction can be observed. To derive the stress σ film parallel to the film surface, the following formula can be used for a hexagonal lattice [135].

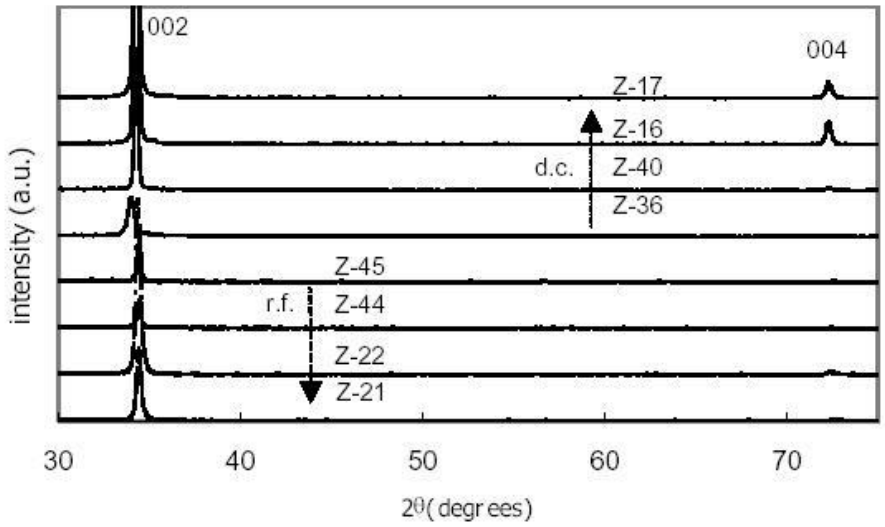

Figure 2.12: *The XRD pattern of the film*

2.10 Characterization Techniques

After the preparation of the samples, different characterization techniques were used to investigate their structure and optical properties. Scanning electron microscope (SEM) was used to get the morphology of the samples. An atomic force microscope (AFM) was utilized to detect the morphology of pre-treated substrates. The detailed information about the structure of the samples can be obtained from XRD measurement. The optical properties were investigated by micro photoluminescence (PL), micro-Raman scattering, and resonant Raman scattering (RRS) measurements. The surface effect versus the diameter of the ZnO nanorods were studied by means of time resolved photoluminescence (TRPL). Here we will briefly describe these techniques.

2.10.1 Scanning Electron Microscope

The scanning electron microscope (SEM) is a type of electron microscope that images the sample surface by scanning it with a high-energy beam of electrons in a raster scan pattern. The electrons interact with the atoms to make the sample producing signals that contain information about the sample's surface topography, composition and other properties such as electrical conductivity. The types of signals produced by a SEM include secondary electrons, back scattered electrons (BSE), characteristic x-rays, light (cathode luminescence), specimen current and transmitted electrons. These types of signal all require specialized detectors for their detection that are not usually all present on a single machine. A scanning electron microscope employs the use of high-energy electrons, rather than photons, to image a surface. The sample must have a moderate electrical conductivity and be stable in a high vacuum environment. It allows direct studying of the surfaces of solid objects and greater depth of focus than the optical microscope. It can hence produce an image that is a good representation of the three-dimensional sample. By heating the metallic filament, a beam of electrons is produced at the top of the microscope. The electron beam traverses a vertical path through the column of the microscope first and then through the electromagnetic lenses that focuses and directs the beam down towards the sample. After hitting the sample, backscattered and secondary electrons are ejected from the sample. Detectors further collect the above emitted electrons and convert them into a signal that is sent to a viewing screen thereby producing an image. The ZnO nanostructure produced by PVD was characterized using SEM. The schematic image of SEM is illustrated in Figure 2.13 in order to show how it works.

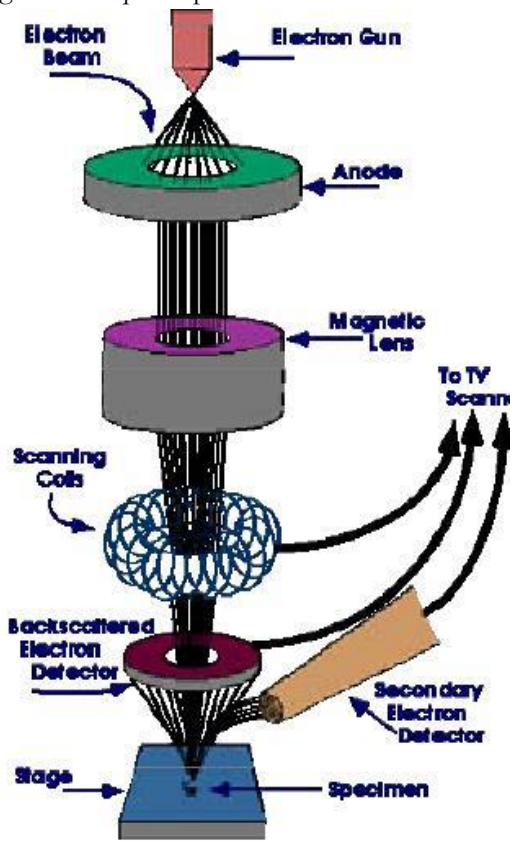

Figure 2.13: *Schematic image of SEM*

The SEM uses electrons instead of light to form an image. A beam of electrons is produced at the top of the microscope by heating of a metallic filament. The electron beam follows a vertical path through the column of the microscope. It makes its way through electromagnetic lenses which focus and direct the beam down towards the samples. Once it hits the sample, other electrons such as backscattered or secondary are ejected from the sample. Detectors collect the secondary or back scattered electrons and convert them to a signal that is sent to a viewing screen similar to the one in an ordinary television, producing an image. To characterize the as-grown ZnO nanostructures, a JEOL JSM-6301F scanning electron microscope was used in our experiments. The chamber pressure was about 10-6 mbar. The gun voltage is 15kV. A max resolution of about 10nm can be achieved. Figure 2.14 gives the typical SEM images of sample. The SEM gives information on the morphology of the surface of the sample, which implies that is possible to determine if any growth has taken place. However, the images from the SEM are not a definitive proof that obtained nanostructures actually consists of ZnO. Even though the SEM produces 3D images they give no information regarding the exact atomic structure of the sample. The 3D images are easy to interpret, and they reveal topographic features of the sample. The SEM images allow us to examine the diameter, length, shape and density of the ZnO nanostructures.

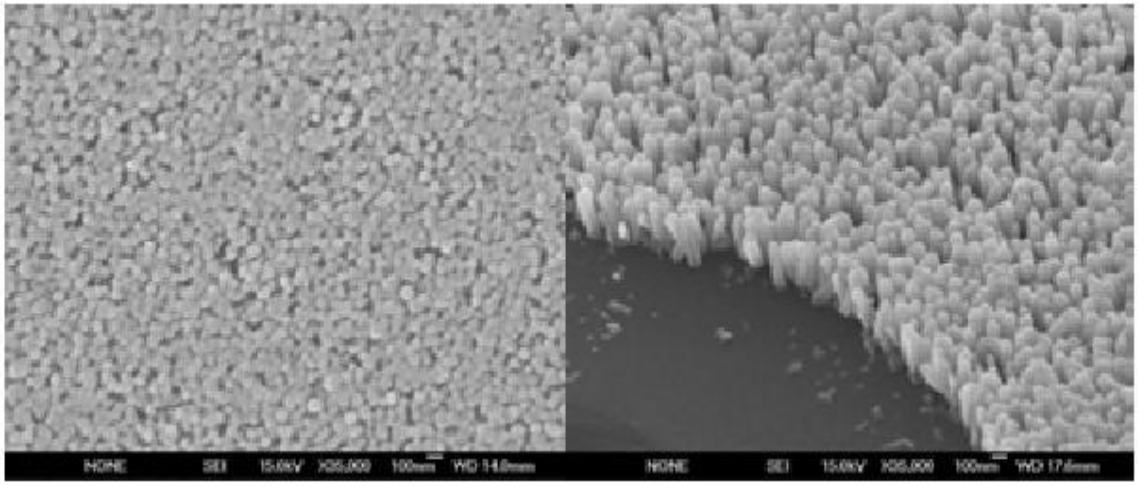

Figure 2.14: *Typical SEM images of ZnO nanorod arrays*

2.10.2 X-ray diffraction

X-rays are electromagnetic radiation of wavelength about 1 Å (10^{-10} m), which is about the same size as an atom. They occur in that portion of the electromagnetic spectrum between gamma-rays and the ultraviolet. The discovery of X-rays in 1895 enabled scientists to probe crystalline structure at the atomic level. When X-rays interact with a crystalline substance (phase), one gets a diffraction pattern. About 95% of all solid materials can be described as crystalline. Each crystalline solid has its unique characteristic X-ray diffraction (XRD) pattern which may be used as a "fingerprint" for its identification. Today about 50,000 inorganic and 25,000 organic single components, crystalline phases, and diffraction patterns have been collected and stored on magnetic or optical media as standards.

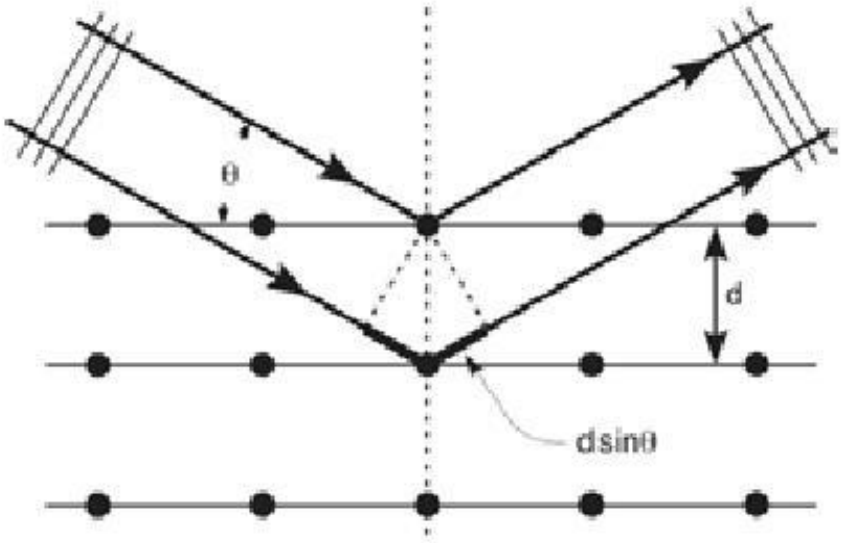

Figure 2.15: *Reflection of x-rays from two planes of atoms in a solid*

Figure 2.15 illustrates the reflection of x-rays from two planes of atoms in a solid. A crystal lattice is a regular three-dimensional distribution (cubic, rhombic, etc.) of atoms in space. These are arranged so that they form a series of parallel planes separated from one another by a distance d, which varies according to the nature of the material. For any crystal, planes exist in a number of different orientations each with its own specific d-spacing. When a monochromatic X-ray beam with wavelength lambda is projected onto a crystalline material at an angle theta, diffraction occurs only when the distance travelled by the rays reflected from successive planes differs by a complete number n of wavelengths, which leads to

Bragg's Law:

$$n\lambda = 2d\sin(\vartheta) \qquad 2.10$$

where *n* is an integer 1,2,3…(usually equal 1), λ is wavelength in angstroms (1.54 Å for copper), d is inter atomic spacing in angstroms, and θ is the diffraction angle in degrees. By varying the angle theta, the Bragg's Law conditions are satisfied by different d-spacing in polycrystalline materials. Plotting the angular positions and intensities of the resultant diffracted peaks of radiation produces a pattern, which is characteristic of the sample. Where a mixture of different phases is present, the resultant diffractogram is formed by addition of the individual patterns. Based on the principle of X-ray diffraction, a wealth of structural, physical and chemical information about the material investigated can be obtained. XRD has been in use in two main areas, for the fingerprint characterization of crystalline materials and the determination of their structure. Once the material has been identified, X-ray crystallography may be used to determine its structure, i.e. how the atoms pack together in the crystalline state and what the inter atomic distance and angle are etc. X-ray diffraction is one of the most important characterization tools used in solid state chemistry and materials science.

One can determine the size and the shape of the unit cell for any compound most easily using the diffraction of x-rays. Figure 2.16 shows the typical XRD pattern of our sample. All the peaks of the XRD patterns can be indexed to ZnO with the hexagonal wurtzite structure. In comparison with the standard card of bulk ZnO with hexagonal structure (see Figure 2.17), no diffraction peaks of other impurities are detected, which testify that the substance deposited on the substrates only belongs to ZnO.

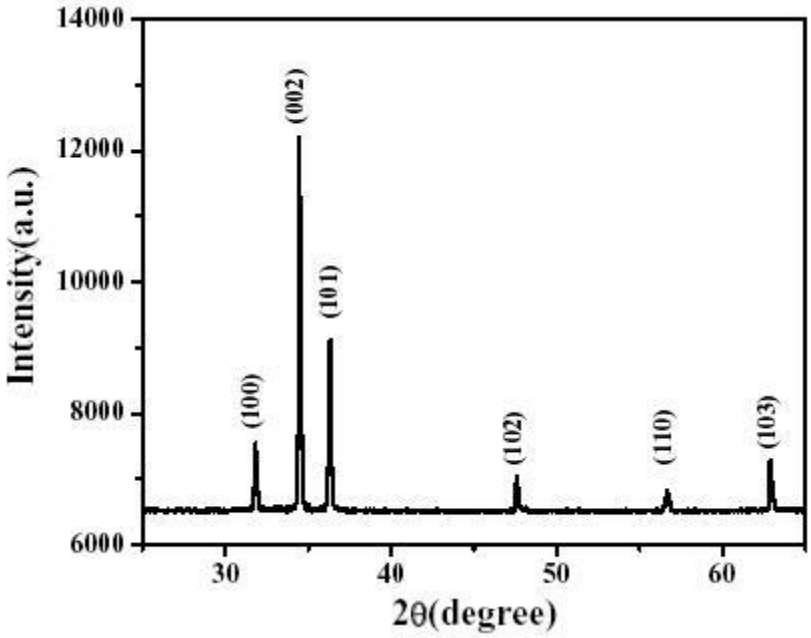

Figure 2.16: *Typical XRD pattern of ZnO nanostructures*

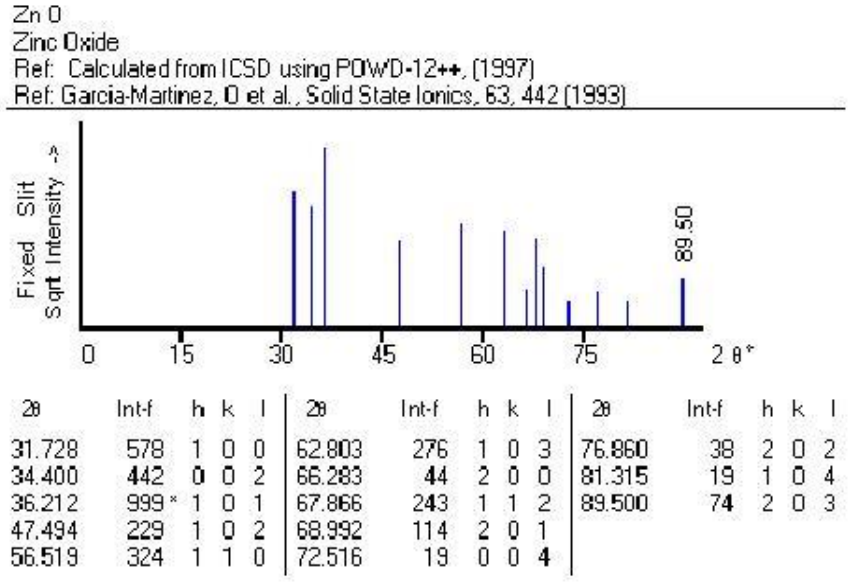

2θ	Int-f	h	k	l	2θ	Int-f	h	k	l	2θ	Int-f	h	k	l
31.728	578	1	0	0	62.803	276	1	0	3	76.860	38	2	0	2
34.400	442	0	0	2	66.283	44	2	0	0	81.315	19	1	0	4
36.212	999 *	1	0	1	67.866	243	1	1	2	89.500	74	2	0	3
47.494	229	1	0	2	68.992	114	2	0	1					
56.519	324	1	1	0	72.516	19	0	0	4					

Figure 2.17: *Standard JCPDS card of bulk ZnO with hexagonal structure*

2.10.3 Atomic force microscope

The atomic force microscope (AFM) is a very high-resolution type of scanning probe microscope, with demonstrated resolution of fractions of a nanometer, more than 1000 times better than the optical diffraction limit. Binnig, Quate and Gerber invented the first AFM in 1986. The AFM is one of the foremost tools for imaging, measuring and manipulating matter at the nanoscale. The term 'microscope' in the name is actually a misnomer because it implies looking, while in fact the information is gathered by "feeling" the surface with a mechanical probe. Piezoelectric elements that facilitate tiny but accurate and precise movements on (electronic) command enable the very precise scanning. Figure 2.18 illustrates the block diagram of AFM.

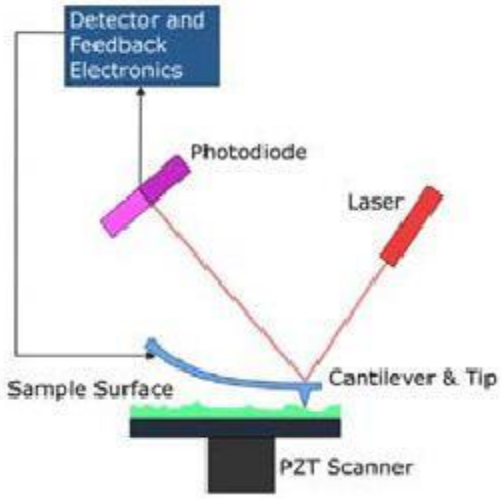

Figure 2.18: *Block Diagram of Atomic Force Microscope*

The AFM consists of a micro scale cantilever with a sharp tip (probe) at its end that is used to scan the specimen surface. The cantilever is typically silicon or silicon nitride with a tip radius of curvature on the order of nanometers. The AFM works by scanning a fine ceramic or semiconductor tip over a surface much the same way as a phonograph needle scans a record. When the tip is brought into proximity of a sample surface, Van der Waals forces between the tip and the sample lead to a deflection of the cantilever. The magnitude of the deflection is captured by a laser that reflects at an oblique angle from the very end of the cantilever. A plot of the laser deflection versus tip position on the sample surface provides the resolution of the hills and valleys that constitute the topography of the surface. The AFM can work with the tip touching the sample (contact mode), or the tip can tap across the surface (tapping mode) much like the cane of a blind person. Compared with SEM, AFM provides extraordinary topographic contrast direct height measurements and unobscured views of surface features. Figure 2.19 shows the 1μm×1μm AFM image of the pre-treated substrates. From this image, it can be seen that the dispersion of ZnO nanoparticles is relatively uniform in the comparison with the nuclei formed on the bare substrates, and the average diameter and height of ZnO nanoparticles on the substrates is about 20nm and 3.5nm respectively. In the comparison between the SEM images of ZnO nanorods and the AFM images of pre-treated Si substrates, the relationship between the sample and seed layer is able to be revealed.

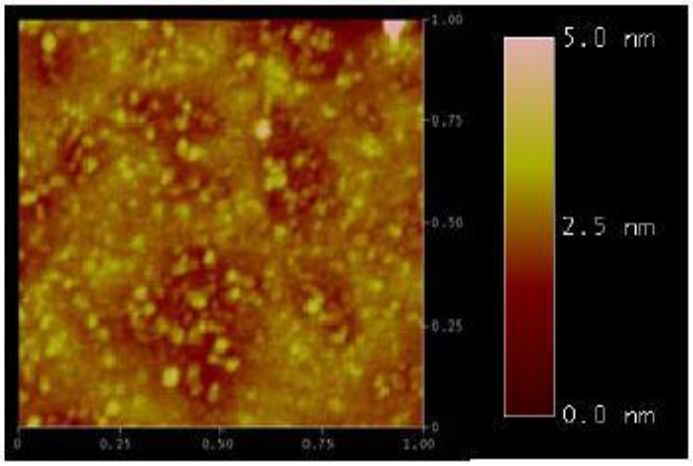

Figure 2.19: *The 1μm×1μm AFM image of the pre-treated substrates*

2.10.4 Transmission Electron Microscope (TEM)

Transmission electron microscopy has been used traditionally as a tool for characterizing local atomic structures of material objects since the information obtained does not require the objects being periodic such as crystal. In the characterization of ZnO nanostructures, TEM is one of the most powerful instruments available due to its excellent imaging and analytical capabilities. TEM imaging allows both the imaging of relatively large areas and the precise measurement. The TEM has a very high magnification and can give detailed information about the structure of even a single nanostructure. The nanostructure appears 'transparent' in the TEM pictures, which enables its measurement more accurately. It is also possible to determine the number of layers in a nanostructure and whether it contains any type of structural damage or irregularities. Another type of interesting observation permitted by the TEM is the shape and location of any residual catalyst that may be incorporated in the nanostructure. One disadvantage with the TEM is that it has to be manually calibrated by taking pictures of special calibration particles several times during each experimental session. The beads have a known size, which is used to compare and calculate the measurements of the particles in the sample.

2.10.5 Field Emission Scanning Electron Microscope

A field-emission cathode in the electron gun of a scanning electron microscope provides narrower probing beams at low as well as high electron energy, resulting in both improved spatial resolution and minimized sample charging and damage. Under vacuum, electrons generated by a Field Emission Source are accelerated in a field gradient. The beam passes through electromagnetic lenses, focusing onto the specimen. As result of this bombardment different types of electrons are emitted from the specimen. A detector catches the secondary electrons and an image of the sample surface is constructed by comparing the intensity of these secondary electrons to the scanning primary electron beam. Finally, the image is displayed on a monitor. The high-resolution reached by FESEM allows the study of very small micro-structural details. FESEM produces clearer, less electro statically distorted images. By FESEM high quality, low voltage images are obtained with negligible

electrical charging of samples. FESEM (FESEM JOEL 7500f) measurements were performed for ZnO nanostructure synthesized by PVD. In this chapter, the overview of synthesis and characterization of ZnO nanostructures is presented. The main applications of se nanostructures are also included in this chapter. In the next chapter, the methodology of my experimental work will be presented.

2.11 References

[1] http://www.answers.com/topic/zinc-oxide 2005, GuruNet Corporation.

[2] Studenikin, S. A., Golego, N., and Cocivera, M., Carrier mobility and density contributions to photoconductivity transients in polycrystalline ZnO films. Journal of Applied Physics, 2000. 87(5): p. 2413-2421.

[3] http://nano-infinity.tradenet.com.tw/application.htm.

[4] http://www.britannica.com/eb/article?tocId=82113, Zinc processing. 2005.

[5] Tran, Nguyen H., Hartmann, Andreas J., and Lamb, Robert N., Structural order of nanocrystalline ZnO films. Journal of Physical Chemistry B, 1999. 103(21): p.4264-4268.

[6] S. Monticone, R. Tufeu, and A.V. Kanaev, J. Phys. Chem. *B,* 1998**,** *102* (16), pp 2854–2862

[7] J.-K. Lee et al, Appl. Phys. Lett. 86, (2005) 183 111.

[8] Shalish I et al., Phys. Rev. B **69**, (2004) 245401

[9] Pearton, S. J., Norton, D. P., Ip, K., Heo, Y. W., and Steiner, T., Recent progress in processing and properties of ZnO. Progress in Materials Science,2005. 50(3): p. 293-340.

[10] Haug, F. J., Geller, Z. S., Zogg, H., Tiwari, A. N., and Vignali, C., Influence of deposition conditions on the thermal stability of ZnO : Al films grown by rf magnetron sputtering. Journal of Vacuum Science and Technology A-Vacuum Surfaces and Films, 2001. 19(1): p. 171-174.

[11] Dogan, Seydi, Ates, Aytunc, Xiong, Gang, Wilkinson, John, Tuzemen, S.,Yildirim, M., and Williams, R.T., Convertibility of conductivity type in reactively sputtered ZnO thin films. Physica Status Solidi (A) Applied Research, 2003. 195(1 SPEC): p. 165-170.

[12] Mirica, Eugenia, Reactive sputter deposition of piezoelectric zinc oxide thin films, in Chemical, Biochemical and Materials Engineering. 2002, Stevens Institute of Technology: New Jersey. p. 175.

[13] Hartmann, A., Puchert, M.K., and Lamb, R.N., Influence of copper dopants on the resistivity of ZnO films. Surface and Interface Analysis, 1996. 24(9): p. 671-674.

[14] Clarke, D. R., Varistor ceramics [Review]. Journal of the American Ceramic Society, 1999. 82(3): p. 485-502.

[15] Jin, B. J., Bae, S. H., Lee, S. Y., and Im, S., Effects of native defects on optical and electrical properties of ZnO prepared by pulsed laser deposition. Materials Science and Engineering B, 2000. 71(1-3): p. 301-305.

[16] Wraback, M., Shen, H., Liang, S., Gorla, C. R., and Lu, Y., High contrast ultrafast optically addressed ultraviolet light modulator based upon optical anisotropy in ZnO films grown on R-plane sapphire. Applied Physics Letters, 1999. 74(4): p. 507-509.

[17] Zu, P., Tang, Z. K., Wong, G. K. L., Kawasaki, M., Ohtomo, A., Koinuma, H., and Segawa, Y., Ultraviolet spontaneous and stimulated emissions from ZnO microcrystallite thin films at room temperature. Solid State Communications, 1997; 103(8): p. 459-463.

[18] Bagnall, D. M., Chen, Y. F., Shen, M. Y., Zhu, Z., Goto, T., and Yao, T., Room temperature excitonic stimulated emission from zinc oxide epilayers grown by plasma-assisted MBE. Journal of Crystal Growth 1998; 184-185: p. 605-609.

[19] Look, D. C., Recent advances in ZnO materials and devices. Materials Science and Engineering B, 2001; 80(1-3): p. 383-387.

[20] Y. Li, G.S. Tompa, S. Liang, C. Gorla, C. Lu and J. Doyle., Transparent and conductive Ga-doped ZnO films grown by low pressure metal organic chemical vapor deposition. Journal of Vacuum Science and Technology A, 1997. 15(3): p. 1663.

[21] Zhang, D. H., Yang, T. L., Ma, J., Wang, Q. P., Gao, R. W., and Ma, H. L., Preparation of transparent conducting ZnO:Al films on polymer substrates by r.f. magnetron sputtering. Applied Surface Science, 2000. 158(1-2): p. 43-48.

[22] Lee, E. Y. M., Tran, N., Russell, J., and Lamb, R. N., Nanocrystalline order of zinc oxide thin films grown on optical fibers. Journal of Applied Physics, 2002. 92(6): p. 2996-2999.

[23] Thornton, J A, High Rate Thick Film Growth. Annual Review of Materials Science, 1977. 7(1): p. 239-260.

[24] Gupta, Vinay and Mansingh, Abhai, Influence of postdeposition annealing on the structural and optical properties of sputtered zinc oxide film. Journal of Applied Physics, 1996. 80(2): p. 1063.

[25] http://www.mrl.ucsb.edu/mrl/centralfacilities/xray/xray-basics/Xraybasics.html#x5. 2005, University of California, Santa Barbara.

[26] Warren, B.E., X-ray Diffraction. 1990: General Publishing Company.

[27] Puchert, M.K., Timbrell, P.Y., and Lamb, R.N., Postdeposition annealing of radio frequency magnetron sputtered ZnO films. Journal of Vacuum Science and Technology A: Vacuum, Surfaces, and Films, 1996. 14(4): p. 2220.

[28] Chu, Sheng-Yuan, Water, Walter, and Liaw, Jih-Tsang, Influence of postdeposition annealing on the properties of ZnO films prepared by RF magnetron sputtering. Journal of the European Ceramic Society, 2003. 23(10): p. 1593-1598.

[29] Moon, Tae-Hyoung, Jeong, Min-Chang, Lee, Woong, and Myoung, Jae-Min, The fabrication and characterisation of ZnO UV detector. Applied Surface Science, 2005. 240(1-4): p. 280-285.

[30] Quintana, M., Ricra, E., Rodriguez, J., and Estrada, W., Spray pyrolysis deposited zinc oxide films for photo-electrocatalytic degradation of methyl orange: influence of the pH. Catalysis Today, 2002. 76(2-4): p. 141-148.

[31] Fang, Guojia J., Li, Dejie, and Yao, Bao-Lun, Influence of post-deposition annealing on the properties of transparent conductive nanocrystalline ZAO

[32] thin films prepared by RF magnetron sputtering with highly conductive ceramic target. Thin Solid Films, 2002. 418(2): p. 156-162.

[32] Burstein, E., Anomalous Optical Absorption Limit in InSb. Physical Review, 1953. 93(3): p. 632-633.

[33] Reynolds, D. C., Look, D. C., Jogai, B., and Morkoc, H., Similarities in the bandedge and deep-centre photoluminescence mechanisms of ZnO and GaN. Solid State Communications, 1997. 101(9): p. 643-646.

[34] Sato, Y. and Sato, S., Preparation and some properties of nitrogen-mixed ZnO thin films. Thin Solid Films, 1996. 281-282(1-2): p. 445-448.

[35] Singh, A. V., Mehra, R. M., Wakahara, A., and Yoshida, A., p-type conduction in codoped ZnO thin films. Journal of Applied Physics, 2003. 93(1): p. 396-399.

[36] Komatsu, M., Ohashi, N., Sakaguchi, I., Hishita, S., and Haneda, H., Ga, N solubility limit in co-implanted ZnO measured by secondary ion mass spectrometry, in Applied Surface Science. 2002. p. 349-352.

[37] D. C. Look, B. Claflin, Ya. I. Alivov, S. J. Park,, The future of ZnO light emitters. physica status solidi (a), 2004. 201(10): p. 2203-2212; 2nd International ZnO workshop, D. C. Look, Editor. 2002: Dayton, Ohio, USA.

[38] Kim, Kyoung-Kook, Kim, Hyun-Sik, Hwang, Dae-Kue, Lim, Jae-Hong, and Park, Seong-Ju, Realization of p-type ZnO thin films via phosphorus doping and thermal activation of the dopant. Applied Physics Letters, 2003. 83(1): p. 63-65.

[39] Lin, Chin-Ching, Chen, San-Yuan, Cheng, Syh-Yuh, and Lee, Hsin-Yi, Properties of nitrogen-implanted p-type ZnO films grown on Si 3N 4/Si by radior frequency magnetron sputtering. Applied Physics Letters, 2005. 84(24): p. 5040- 5042.

[40] Guo, Xin-Li, Tabata, Hitoshi, and Kawai, Tomoji, Pulsed laser reactive deposition of p-type ZnO film enhanced by an electron cyclotron resonance source. Journal of Crystal Growth, 2001. 223(1-2): p. 135-139.

[41] Look, D. C., Reynolds, D. C., Litton, C. W., Jones, R. L., Eason, D. B., and Cantwell, G., Characterisation of homoepitaxial p-type ZnO grown by molecularbeam epitaxy. Applied Physics Letters, 2002 81(10): p. 1830-1832.

[42] Lu, J. G., Ye, Z. Z., Zhuge, F., Zeng, Y. J., Zhao, B. H., and Zhu, L. P., p-type conduction in N--Al co-doped ZnO thin films. Applied Physics Letters, 2004 85(15): p. 3134-3135.

[43] Joseph, M., Tabata, H., Saeki, H., Ueda, K., and Kawai, T., Fabrication of the low-resistive p-type ZnO by codoping method. Physica B: Condensed Matter, 2001. 302-303: p. 140-148.

[44] Bian, J. M., Li, X. M., Gao, X. D., Yu, W. D., and Chen, L. D., Deposition and electrical properties of N--In codoped p-type ZnO films by ultrasonic spray pyrolysis. Applied Physics Letters, 2004. 84(4): p. 541-543.

[45] Li, B.S., Liu, Y.C., Shen, D.Z., Lu, Y.M., Zhang, J.Y., Fan, X.W., Zhi, Z.Z., Mu, R.X., and Henderson, D.O., Optical properties and electrical characterisation of p-type zno thin films prepared by thermally oxiding Zn3N2 thin films. Journal of Materials Research, 2003. 18(1): p. 8-13.

[46] Wang, Jinzhong, Du, Guotong, Zhao, Baijun, Yang, Xiaotian, Zhang, Yuantao, Ma, Yan, Liu, Dali, Chang, Yuchun, Wang, Haisong, Yang, Hongjun, and Yang, Shuren, Epitaxial growth of NH3-doped ZnO thin films on oriented sapphire substrates. Journal of Crystal Growth, 2003. 255(3-4): p. 293-297.

[47] Li, X., Yan, Y., Gessert, T. A., Perkins, C. L., Young, D., DeHart, C., Young, M., and Coutts, T. J. Chemical vapor deposition-formed p-type ZnO thin films. In Papers from the 49th International Symposium of the American Vacuum Society. 2003: AVS.

[48] http://www.nanotec.org.uk/.

[49] Cao, Guozhong, Nanostructures and nanomaterials: synthesis, properties and applications. 2004, London: Imperial College Press.

[50] Ramamoorthy, K., Sanjeeviraja, C., Jayachandran, M., Sankaranarayanan, K., Ganesan, V., Misra, Pankaj, and Kukreja, L.M., A novel nano-architecture for ZnO thin films on Si, GaAs and InP single crystal wafers by L-MBE as value in nano-robotic (machining) device fabrication efforts. Materials Science in Semiconductor Processing, 2005. 8(4): p. 555-563.

[51] Radoi, R., Fernandaacute;ndez, P., Piqueras, J., Wiggins, M. S., and Solis, J., Luminescence properties of mechanically milled and laser irradiated ZnO. Nanotechnology, 2003(7): p. 794-798.

[52] Xie, Qin, Dai, Zhou, Liang, Jianbo, Xu, Liqiang, Yu, Weichao, and Qian, Yitai, Synthesis of ZnO three-dimensional architectures and their optical properties, in Solid State Communications.

[53] Huang, Michael H., Mao, Samuel, Feick, Henning, Yan, Haoquan, Wu, Yiying, Kind, Hannes, Weber, Eicke, Russo, Richard, and Yang, Peidong, Room- Temperature Ultraviolet Nanowire Nanolasers. Science, 2001. 292(5523): p. 1897-1899.

[54] Pan, Zheng Wei, Dai, Zu Rong, and Wang, Zhong Lin, Nanobelts of Semiconducting Oxides. Science, 2001. 291(5510): p. 1947-1949.

[55] Kong, Xiang Yang, Ding, Yong, Yang, Rusen, and Wang, Zhong Lin, Single-Crystal Nanorings Formed by Epitaxial Self-Coiling of Polar Nanobelts. Science, 2004. 303(5662): p. 1348-1351.

[56] Hu, P., Liu, Y., Wang, X., Fu, L., and Zhu, D., Tower-like structure of ZnO nanocolumns. Chemical Communications, 2003. 9(11): p. 1304-1305.

[57] Lao, J.Y., Huang, J.Y., Wang, D.Z., and Ren, Z.F., ZnO nanobridges and nanonails. Nano Letters, 2003. 3(2): p. 235-238.

[58] Wang, Z., Qian, X.-F., Yin, J., and Zhu, Z.-K., Large-Scale Fabrication of Tower-like, Flower-like, and Tube-like ZnO Arrays by a Simple Chemical Solution Route. Langmuir, 2004. 20(8): p. 3441-3448.

[59] Willander, M., Nur, O., Lozovik, Yu E., Al-Hilli, S.M., Chiragwandi, Z., Hu, Q.- H., Zhao, Q.X., and Klason, P., Solid and soft nanostructured materials:

[60] Huang, M.H., Mao, S., Feick, H., Haoquan, Yan, Yiying, Wu, Kind, H., Weber, E., Russo, R., and Peidong, Yang, Room-temperature ultraviolet nanowire nanolasers. Science, 2001. 292(5523): p. 1897-1899.

[61] Heutz, Sandrine, Salvan, Georgeta, Jones, Tim S., and Zahn, Dietrich R.T., Effects of annealing on the properties of molecular thin film heterostructures. Advanced Materials, 2003. 15(13): p. 1109-1112.

[62] Norton, D. P., Heo, Y. W., Ivill, M. P., Ip, K., Pearton, S. J., Chisholm, M. F., and Steiner, T., ZnO: growth, doping and processing. Materials Today, 2004. 7(6): p. 34-40.

[63] Zeng, Hao, Li, Jing, Liu, J. P., Wang, Zhong L., and Sun, Shouheng, Exchangecoupled nanocomposite magnets by nanoparticle self-assembly. 2002. 420(6914): p. 395-398.

[64] Gao, Pu Xian, Lao, Chang Shi, Hughes, William L., and Wang, Zhong L., Three-dimensional interconnected nanowire networks of ZnO. Chemical Physics Letters, 2005. 408(1-3): p. 174-178.

[65] Li, Y., Meng, G. W., Zhang, L. D., and Phillipp, F., Ordered semiconductor ZnO nanowire arrays and their photoluminescence properties. Applied Physics Letters, 2000. 76(15): p. 2011-2013.

[66] Liu, B. and Hua, C.Z., Fabrication of ZnO "Dandelions" via a modified Kirkendall process. Journal of the American Chemical Society, 2004. 126(51): p. 16744-16746.

[67] Mo, M., Yu, J.C., Zhang, L., and Li, S.-K.A., Self-assembly of ZnO nanorods and nanosheets into hollow microhemispheres and microspheres, in Advanced Materials. 2005. p. 756-760.

[68] Gao, P.X. and Wang, Z.L., Mesoporous polyhedral cages and shells formed by textured self-assembly of ZnO nanocrystals. Journal of the American Chemical Society, 2003. 125(37): p. 11299-11305.

[69] Tian, Z.R., Voigt, J.A., Liu, J., Mckenzie, B., Mcdermott, M.J., Rodriguez, M.A., Konishi, H., and Xu, H., Complex and oriented ZnO nanostructures. Nature Materials, 2003. 2(12): p. 821-826.

[70] Liu, B. and Zeng, H.C., Room temperature solution synthesis of monodispersed single-crystalline ZnO nanorods and derived hierarchical nanostructures. Langmuir, 2004. 20(10): p. 4196-4204.

[71] W.I. Park, G.-C. Yi, M. Kim, S.J. Pennycook,, ZnO Nanoneedles Grown Vertically on Si Substrates by Non-Catalytic Vapor-Phase Epitaxy. Advanced Materials, 2002. 14(24): p. 1841-1843.

[72] Gao, Pu Xian, Ding, Yong, Mai, Wenjie, Hughes, William L., Lao, Changshi, and Wang, Zhong Lin, Conversion of Zinc Oxide Nanobelts into Superlattice- Structured Nanohelices. Science, 2005. 309(5741): p. 1700-1704.

[73] Hughes, W.L. and Wang, Z.L., Formation of Piezoelectric Single-Crystal Nanorings and Nanobows. J. Am. Chem. Soc., 2004. 126(21): p. 6703-6709.

[74] Kucheyev, S. O., Williams, J. S., and Jagadish, C., Ion-beam-defect processes in group-III nitrides and ZnO. Vacuum, 2004. 73(1): p. 93-104.

[75] Yamamoto, T., Codoping for the fabrication of p-type ZnO. Thin Solid Films, 2002. 420-421(Complete): p. 100-106.

[76] Miyakawa, M., Ueda, K., and Hosono, H., Carrier control in transparent semiconducting oxide thin films by ion implantation: MgIn2O4 and ZnO Nuclear Instruments and Methods in Physics Research Section B: Beam Interactions with Materials and Atoms, 2002. 191(1-4): p. 173-177.

[77] Jeong, T. S., Han, M. S., Youn, C. J., and Park, Y. S., Raman scattering and photoluminescence of As ion-implanted ZnO single crystal. Journal of Applied Physics, 2004. 96(1): p. 175-179.

[78] Ip, K., Overberg, M. E., Heo, Y. W., Norton, D. P., Pearton, S. J., Kucheyev, S. O., Jagadish, C., Williams, J. S., Wilson, R. G., and Zavada, J. M., Thermal stability of ion-implanted hydrogen in ZnO. Applied Physics Letters, 2002. 81(21): p. 3996-3998.

[79] Kucheyev, S. O., Jagadish, C., Williams, J. S., Deenapanray, P. N. K., Yano, Mitsuaki, Koike, Kazuto, Sasa, Shigehiko, Inoue, Masataka, and Ogata, Kenichi, Implant isolation of ZnO. Journal of Applied Physics, 2003. 93(5): p. 2972- 2976.

[80] http://composite.about.com/od/referencematerials/l/blpreface.htm, Composites/Plastics. 2005, About Inc.

[81] Hu, You-Hua, Gao, Hui, Yan, Feng-Yuan, Liu, Wei-Min, and Qi, Chen-Ze, Tribological and mechanical properties of nano ZnO-filled epoxy resin composites. Mocaxue Xuebao/Tribology, 2003. 23(3): p. 216-220.

[82] Toutorski, I.A., Tkachenko, T.E., Pokidko, B.V., Maliavski, N.I., and Sidorov, V.I., Mechanical properties and structure of zinc-containing latex-silicate composites. Journal of Sol-Gel Science and Technology, 2003. 26(1-3): p. 505- 509.

[83] Schwartz., Mel and Upper Saddle River, N.J., Composite materials. 1997 Prentice Hall PTR.

[84] http://www.courses.ahc.umn.edu/medicalschool/BMEn/5001/notes/composites.htm Introduction to Composite Materials. 1999.

[85] P. Gao, "Piezoelectric Nanostructures of Zinc Oxide: Synthesis, Characterization, and Devices," in School of Materials Science and Engineering, vol. Ph.D. Atlanta: Georgia Institute of Technology, 2005, pp. 269.

[86] D. C. Agarwal, R. S. Chauhan, A. Kumar, D. Kabiraj, F. Singh, S. A. Khan, D. K. Avasthi, J. C. Pivin, M. Kumar, J. Ghatak, and P. V. Satyam, "Synthesis and characterization of ZnO thin film grown by electron beam evaporation," Journal of Applied Physics, vol. 99, 2006.

[87] Z. L. Wang, X. Y. Kong, Y. Ding, P. X. Gao, W. L. Hughes, R. S. Yang, and Y. Zhang, "Semiconducting and piezoelectric oxide nanostructures induced by polar surfaces," Advanced Functional Materials, vol. 14, pp. 943-956, 2004.

[88] Z. L. Wang, "Self-assembled nanoarchitectures of polar nanobelts/nanowires," Journal of Materials Chemistry, vol. 15, pp. 1021-1024, 2005.

[89] W. Tjhen, T. Tamagawa, C.-P. Ye, C.-C. Hsueh, P. Schiller, and D. L. Polla, Micro Electro Mechanical Systems Proceedings, pp. 114, 1991.

[90] T. Nakamura, H. Minoura, and H. Muto, "Fabrication of ZnO (0001) epitaxial films on the cubic (111) substrate with C6 symmetry by pulsed laser deposition," Thin Solid Films, vol. 405, pp. 109-116, 2002.

[91] Y. Sun, G. M. Fuge, and M. N. R. Ashfold, "Growth of aligned ZnO nanorod arrays by catalyst-free pulsed laser deposition methods," Chemical Physics Letters, vol. 396, pp. 21-26, 2004.

[92] Y. Sun, G. M. Fuge, and M. N. R. Ashfold, "Growth mechanisms for ZNO nanorods formed by pulsed laser deposition," Superlattices and Microstructures, vol. 39, pp. 33-40, 2006.

[93] C. H. Bae, S. M. Park, S. C. Park, and H. S. Ha, "Array of ultraviolet luminescent ZnO nanodots fabricated by pulsed laser deposition using an anodic aluminum oxide template," Nanotechnology, vol. 17, pp. 381-384, 2006.

[94] B. Zheng, C. Lu, G. Gu, A. Makarovski, G. Finkelstein, and J. Liu, vol. 2, pp. 895, 2002.

[95] C. M. Lieber and X. F. Duan, Advanced Materials, vol. 12, pp. 298, 2000.

[96] K. Haga, M. Kamidaira, Y. Kashiwaba, T. Sekiguchi, and H. Watanabe, Journal of Crystal Growth, vol. 214-215, pp. 77-80, 2000.

[97] S. Jain, T. T. Kodas, and M. Hampden-Smith, "Synthesis of ZnO Thin Films by Metal-Organic CVD of Zn(CH3COO)2," Chemical Vapor Deposition, vol. 4, pp. 51-59, 1998.

[98] S. Muthukumar, H. Sheng, J. Zhong, Z. Zhang, N. W. Emanetoglu, and Y. Lu, "Selective MOCVD Growth of ZnO Nanotips," IEEE Transactions on Nanotechnology, vol. 2, pp. 50-54, 2003.

[99] S.-W. Kim, S. Fujita, and S. Fugita, "ZnO nanowires with high aspect ratios frown by metalorganic chemical vapor depostion using gold nanoparticles," Applied Physics Letters, vol. 86, 2005.

[100] B. P. Zhang, N. T. Binh, K. Wakatuki, Y. Segawa, Y. Yamada, N. Usami, M. Kawasaki, and H. Koinuma, Applied Physics Letters, vol. 84, pp. 4098-4100, 2004.

[101] K. Nakahara, H. Takasu, P. Fons, K. Iwata, A. Yamada, K. Matsubara, R. Hunger, and S. Niki, "Growth and characterization of undoped ZnO films for single crystal based device use by radical source molecular beam epitaxy (RS-MBE) " Journal of Crystal Growth, vol. 227-228, pp. 923-928, 2001.

[102] V. A. Fonoberov and A. A. Baladin, "Origin of ultraviolet photoluminescence in ZnO quantum dots: Confined excitons versus surface-bound impurity exciton complexes," Applied Physics Letters, vol. 85, pp. 5971-5973, 2004.

[103] S. M. George, A. W. Ott, and J. W. Klaus, "Surface Chemistry for Atomic Layer Growth," Journal of Physical Chemistry, vol. 100, pp. 13231, 1996.

[104] M. Scharrer, X. Wu, A. Yamilov, H. Cao, and R. P. H. Chang, "Fabrication of inverted opal ZnO photonic crystals by atomic layer deposition," Applied Physics Letters, vol. 86, pp. 1-3, 2005.

[105] N. Hoivik, J. W. Elam, S. M. George, K. C. Gupta, V. M. Bright, and Y. C. Lee, "Atomic layer deposition (ALD) technology for reliable MEMS," Microwave Symposium Digest, 2002 IEEE MIT-S International, pp. 1129-1232, 2002.

[106] H. Q. Lee, S. J. Chua, K. P. Loh, E. A. Fitzgerald, and Y. W. Koh, "Synthesis an optical properties of well aligned ZnO nanorods on GaN by hydrothermal synthesis," Nanotechnology, vol. 17, pp. 483-488, 2006.

[107] H. J. Chang, C. Z. Lu, Y. Wang, C.-S. Son, S.-I. Kim, Y.-H. Kim, and I.-H. Choi, "Optical properties of ZnO nanocrystals synthesized by using sol-gel method," Journal of the Korean Physical Society, vol. 45, pp. 959-962, 2004.

[108] D. Bao, A. Kuang, and H. Gu, "Sol-gel-derived c-axis oriented ZnO thin films," Thin Solid Films, vol. 312, pp. 37-39, 1998.

[109] S. E. Ahn, J. S. Lee, K. Kim, S. Kim, B. H. Kang, K. H. Kim, and G. T. Kim, "Photoresponse of sol-gel-synthesized ZnO nanorods," Applied Physics Letters, vol. 84, pp. 5022-5024, 2004.

[110] M. G. Scientific, "High Temperature 54500 Barnstead Thermolyne Furnace," in www.mgscientific.com/store. Pleasant Prairie, WI (08/2006).

[111] J. H. Song, X. D. Wang, E. Riedo, and Z. L. Wang, "Systematic study on experimental conditions for large-scale growth of aligned ZnO nanowires on nitrides," Journal of Physical Chemistry B, vol. 109, pp. 9869-9872, 2005.

[112] C. Ma, "Systematic investigation on the growth of one-dimensional wurtzite nanostructures," in School of Materials Science and Engineering, vol. Ph.D. Atlanta: Georgia Institute of Technology, 2005.

[113] H. L. Cobb, "Cadmium Whiskers," Monthly Review of the American Electroplaters Society, vol. 33, pp. 28-30, 1946.

[114] K. G. Compton, A. Mendizza, and S. M. Arnold, "Filamentary Growths on Metal Surfaces-Whiskers," Corrosion, vol. 7, pp. 327-334, 1951

[115] C. Herring and J. K. Galt, Physics Review, vol. 85, pp. 1069, 1952.

[116] M. O. Peach, "Mechanism of Growth of Metal Whiskers," Journal of Applied Physics vol. 23, pp. 1401, 1952.

[117] S. E. Koonce and S. M. Arnold, "Growth of Metal Whiskers," Journal of Applied Physics (letters to the editor), vol. 24, pp. 365-366, 1954.

[118] F. C. Frank, "On Tin Whiskers," Phil. Mag., vol. XLIV, pp. 854-860, 1953.

[119] J. D. Eshelby, "A Tentative Thoery of Metallic Whisker Growth," Physical Review, vol. 91, pp. 755-756, 1953

[120] S. Amelinckx, W. Bontinck, W. Dekeyser, and F. Seitz, "On the Formation and Properties of Helical Dislocations," Phil. Mag., vol. 82, pp. 355-377, 1957.

[121] G. W. Sears, "A Growth Mechanism for Mercury Whiskers," Acta Metallurgica, vol. 3, pp. 361-366, 1955.

[122] J. M. Blakely and K. A. Jackson, "Growth of Crystal Whiskers," Journal of Chemical Physics, vol. 37, pp. 428, 1962 .

[123] Y. N. Xia, P. D. Yang, Y. G. Sun, Y. Y. Wu, B. Mayers, B. Gates, Y. D. Yin, F. Kim, and Y. Q. Yan, "2003," Advanced Materials, vol. 15, pp. 353-389.

[124] Z. R. Dai, Z. W. Pan, and Z. L. Wang, "Novel nanostructures of functional oxides synthesized by thermal evaporation," Advanced Functional Materials, vol. 13, pp. 9-24, 2003.

[125] Quaranta. F., Valentini, A., Rizzi, F.R. and Casamassima, G., Dual-ion-beam Sputter Deposition of ZnO films. Journal of Applied Physics, 1993. 74(1): p. 244-248.

[126] Fang, Guojia J., Li, Dejie, and Yao, Bao-Lun, Influence of post-deposition annealing on the properties of transparent conductive nanocrystalline ZAO thin films prepared by RF magnetron sputtering with highly conductive ceramic target. Thin Solid Films, 2002. 418(2): p. 156-162.

[127] Dogan, Seydi, Ates, Aytunc, Xiong, Gang, Wilkinson, John, Tuzemen, S., Yildirim, M., and Williams, R.T., Convertibility of conductivity type in reactively sputtered ZnO thin films. Physica Status Solidi (A) Applied Research, 2003.195(1 SPEC): p. 165-170.

[128] Haug, F. J., Geller, Z. S., Zogg, H., Tiwari, A. N., and Vignali, C., Influence of deposition conditions on the thermal stability of ZnO : Al films grown by rf magnetron sputtering. Journal of Vacuum Science and Technology A-Vacuum Surfaces and Films, 2001. 19(1): p. 171-174.

[129] Yang, Xiaotian, Du, Guotong, Wang, Xinqiang, Wang, Jinzhong, Liu, Boyang, Zhang, Yuantao, Liu, Dan, Liu, Dali, Yang, Shuren, and Ong, H.C., Effect of post-thermal annealing on properties of ZnO thin film grown on Al_2O_3 by metal-organic chemical vapor deposition.Journal of Crystal Growth, 2003. 252(1-3): p. 275-278.

[130] Hao, X. T., Ma, J., Zhang, D. H., Yang, T. L., Ma, H. L., Yang, Y. G., Cheng, C. F., and Huang, H., Thickness dependence of structural, optical and electrical properties of ZnO : Al films prepared on flexible substrates. Applied Surface Science, 2002. 189(1-2): p. 18-23.

[131] Park, K. C., Ma, D. Y., and Kim, K. H., The Physical Properties of Al-Doped Zinc Oxide Films Prepared by Rf Magnetron Sputtering. Thin Solid Films, 1997. 305(1-2): p. 201-209.

[132] Uthanna, S., Subramanyam, T. K., Srinivasulu Naidu, B., and Mohan Rao, G. Structure-composition-property dependence in reactive magnetron sputtered ZnO thin films. Optical Materials, 2002. 19(4): p. 461-469.

[133] Jayaraj, M. K., Antony, A., and Ramachandran, M., Transparent conducting zinc oxide thin film prepared by off-axis rf magnetron sputtering. Bulletin of Materials Science (India), 2002. 25(3): p. 227-230.

[134] Gupta, Vinay and Mansingh, Abhai, Influence of postdeposition annealing on the structural and optical properties of sputtered zinc oxide film. Journal of Applied Physics, 1996. 80(2): p. 1063.

[135] Cebulla, R., Wendt, R., and Ellmer, K., Al-doped zinc oxide films deposited by simultaneous rf and dc excitation of a magnetron plasma: relationships between plasma parameters and structural and electrical film properties. Journal of Applied Physics, 1998. 83(2): p. 1087.

[136] Z.L. Wang, Materials Today, 7 (2004) 25-33.

[137] R. B. Peterson, C. L. Fields and B. A. Gregg, Langmuir 20 (2004) 5114-118.

[138] Y. Tak and K. Yong, J. Phys. Chem. B 109 (2005)19263-19269.

[139] C. H. Hung and W. T. Whang, J. Cryst. Growth 268 (2004) 242-248.

[140] X. J. Feng, L. Feng, M. H. Jin, J. Zhai and L. Jiang, J. Am. Chem. Soc. 126 (2004) 62-63.

[141] Y. Tak and K. Yong, J. Phys. Chem. B 109 (2005)19263-19269.

[142] C. H. Hung and W. T. Whang, J. Cryst. Growth 268 (2004) 242-248.

[143] X. J. Feng, L. Feng, M. H. Jin, J. Zhai and L. Jiang, J. Am. Chem. Soc. 126 (2004) 62-63.